Isotope variability in daily sampled precipitation in Reykjavík and its connection to climate parameters

Rósa Ólafsdóttir

Faculty of Earth Sciences
University of Iceland
2020

Isotope variability in daily sampled precipitation in Reykjavík and its connection to climate parameters

Rósa Ólafsdóttir

60 ECTS thesis submitted in partial fulfillment of a
Magister Scientiarum degree in Environment and Natural Resources

MS Committee
Árný Erla Sveinbjörnsdóttir
Hans Christian Steen-Larsen

Master's Examiner
Þröstur Þorsteinsson

Faculty of Earth Sciences
School of Engineering and Natural Sciences
University of Iceland
Reykjavik, June 2020

Isotope variability in daily sampled precipitation in Reykjavík and its connection to climate parameters
Isotope variability in precipitation and climate
60 ECTS thesis submitted in partial fulfillment of a *Magister Scientiarum* degree in Environment and Natural Resources

Faculty of Earth Sciences
School of Engineering and Natural Sciences
University of Iceland
Sturlugata 7
101 Reykjavik
Iceland

Telephone: 525 4000

Bibliographic information:
Rósa Ólafsdóttir, 2020, *Isotope variability in daily sampled precipitation in Reykjavík and its connection to climate parameters*, Master's thesis, Faculty of Earth Sciences, University of Iceland, pp. 64.

Printing: Háskólaprent
Reykjavik, Iceland, June 2020

Abstract

Stable water isotopes ($\delta^{18}O$ and δD) in precipitation can help to understand hydrological and atmospheric processes within the water cycle. While long-term monthly precipitation isotope datasets are available, limited data exists on daily precipitation samples. In this study isotopic values of daily precipitation from 30 June 2016 to 17 February 2020 sampled in Reykjavík are reported and interpreted in relation to weather data from the Icelandic Meteorological Office (IMO). A large range in $\delta^{18}O$ (-17.48 to -0.67‰), δD (-132.3 to +1.3‰) and the *d*-excess ($d = \delta D - 8\delta^{18}O$) (-7.5 to +31.4‰) values was observed in the daily precipitation data. Significant anti-correlation was observed between *d*-excess and temperature (r = -0.61 ± 0.05) and specific humidity (r = -0.56 ± 0.05). Weaker correlation was found between isotopic values ($\delta^{18}O$) and the above meteorological parameters (r = 0.26 ± 0.05 and 0.22 ± 0.05). Some differences were also observed when correlations were studied by seasons. Results from sampling a low-pressure front passing Reykjavík (12 samples) show large isotopic inter variability that can be correlated with temperature and specific humidity. Moderate correlation is found between the observed isotopic data and the isotope-enabled ECHAM5-wiso climate model. The model's parametrization of precipitation could be improved by taking into consideration higher resolution isotope data. Relationship between the isotopic precipitation data and the North Atlantic Oscillation (NAO) suggests anti-correlation between $\delta^{18}O$ (and δD) and the NAO index, especially during winter months, though statistically non-significant. Database with results from water isotope measurements performed at the Institute of Earth Sciences since 2006 was constructed, to facilitate available water isotopic data for future research.

Útdráttur

Stöðugar samsætur súrefnis ($\delta^{18}O$) og vetnis (δD) í úrkomu geta hjálpað til við að skilja ýmis ferli vatnshringrásarinnar. Alþjóðlegur gagnagrunnur um samsætur úr mánaðar úrkomusýnum er tiltækur, en niðurstöður fyrir daglega safnaða úrkomu eru af skornum skammti og engar slíkar eru til fyrir Ísland. Í þessari rannsókn er greint frá samsætumælingum á daglega safnaðri úrkomu í Reykjavík frá 30. júní 2016 til 17. febrúar 2020 og túlkun þeirra með tilliti til veðurfarsgagna frá Veðurstofu Íslands (VÍ). Mikill breytileiki mælist í daglegum gildum $\delta^{18}O$ (-17,48 til -0,67‰), δD (-132,3 til 1,3‰) og tvívetnisauka ($d = \delta D - 8\delta^{18}O$) (-7.5 to +31.4‰). Marktæk neikvæð fylgni fannst milli tvívetnisaukans og hitastigs (r = -0.61 ± 0.05) og eðlisraka (r = -0.56 ± 0.05). Veikari fylgni mældist milli samsætugilda ($\delta^{18}O$) og fyrrgreindra veðurfarsþátta og er hún mismunandi mikil eftir árstíðum. Niðurstöður sýnatöku á 30 mínútna fresti úr lægð sem gekk hratt yfir Reykjavík sýna mikinn breytileika á samsætugildum, sem hægt er að tengja breytingum á hitastigi og eðlisraka. Samanburður á mældum gögnum við gögn úr loftslagslíkaninu ECHAM5-wiso, sem tekur inn samsætur við mat á úrkomu, sýnir að meiri upplausn í samsætugögnum myndi betrumbæta líkanið, sérstaklega hvað varðar tvívetnisaukann. Samband milli samsætugagna daglegra úrkomusýna og Norður-Atlantshafs-sveiflunnar (NAO) benda til neikvæðrar fylgni milli $\delta^{18}O$ (og δD) og NAO-vísis, sérstaklega yfir vetrarmánuðina. Sú fylgni er þó ekki tölfræðilega marktæk. Verkefnið fól einnig í sér gerð gagnagrunns með öllum niðurstöðum samsætumælinga við Jarðvísindastofnun Háskólans frá 2006, til að auðvelda notkun gagnanna við frekari rannsóknir.

Table of Contents

List of Figures

List of Tables

Abbreviations

CRDS = Cavity Ring Down Spectroscopy

ECMWF = European Centre for Medium-Range Weather Forecasts

GCM = General Circulation Model

GNIP = Global Network of Isotopes in Precipitation

IAEA = International Atomic Energy Agency

IES = Institute of Earth Sciences

IRMS = Isotope Ratio Mass Spectrometer

MWL = Meteoric Water Line

GMWL = Global Meteoric Water Line / LMWL = Local Meteoric Water Line

NAO = North Atlantic Oscillation

SDPA = Standard Deviation for Proficiency Assessment

VSMOW = Vienna Standard Mean Ocean Water

WMO = World Meteorological Organization

WICO = Water Isotope Inter-Comparison

a.s.l. = above sea level

D = deuterium

δ = scaled isotopic value

‰ = promil, parts per thousand

d = deuterium excess

r = correlation coefficient

SD = Standard deviation

DJF = December, January, February

MAM = March, April, May

JJA = June, July, August

SON = September, October, November

Acknowledgements

I would like to thank the Institute of Earth Science for the opportunity to do this research alongside my work at the institute, the use of facilities and technical support from Þorsteinn Jónsson.

Helga Ívarsdóttir at the Icelandic Meteorological Office for her help with the meteorological data and more importantly for the moral support provided throughout this project. I also want to thank Hera Guðlaugsdóttir, who started the precipitation collection in 2016, for her part in the sampling and other valuable input.

A very special thanks to my family, my husband Andri and my children, Alda Björk and Arnar Logi, for their patience, love, and endless support. I could not have finished this without them.

Last but not least I would like to thank my supervisors for their support and motivation through this project: Árný Erla Sveinbjörnsdóttir for her expert guidance, for always having time to answer my questions and for encouraging me to continue working and Hans Christian Steen-Larsen for his help with the data and interpretation.

1 Introduction

Global climate change has occurred over the last 150 years that can be attributed to anthropogenic greenhouse gas emission (Stocker et al., 2013). The atmospheric hydrological cycle is a major component of the climate system, mainly due to its role of positive feedback mechanism from water vapor and clouds (Bony et al., 2006; Held & Soden, 2006). Ecosystems and human societies are very sensitive to climate change (Stocker et al., 2013). Intensification of the water cycle may lead to changes in water-resource availability, lead to amplification of warming through the water vapor feedback and it could increase the frequency and intensity of tropical storms, floods, and droughts (Held & Soden, 2006). By studying water isotopes in precipitation, the physical processes governing the isotopic composition in the atmospheric water cycle can be revealed. This is not only important to improve the prediction of future climate variability by isotope-enabled General Circulation Models (GCMs), but also for enhanced understanding of the isotope signal in ice-cores. Improved understanding of the Earth's water cycle is also a key element of global efforts to develop policies and practices for the sustainable management of water resources.

The isotopic composition of precipitation varies un multiple temporal and spatial scales due to fractionation of water isotopes during evaporation, condensation, and exchange within the hydrologic cycle. The main factors controlling the oxygen and hydrogen isotope variation in precipitation include surface temperature in mid and high latitudes (Dansgaard, 1964), precipitation amount in the tropics (Dansgaard, 1964; Rozanski, Araguás-Araguás, & Gonfiantini, 1993), convective activity (Risi, Bony, & Vimeux, 2008), altitude (Gonfiantini, Roche, Olivry, Fontes, & Zuppi, 2001) and the moisture source (Balagizi, Kasereka, Cuoco, & Liotta, 2018; Sjostrom & Welker, 2009; Soderberg et al., 2013).

The lack of precipitation isotope data has been a limitation for comprehensive evaluation of climatic factors and sources of moisture in different parts of the world. So far, global precipitation isotopes have only been monitored on a monthly time scale by Global Network for Isotopes in Precipitation (GNIP), which has been operated by the International Atomic Energy Agency (IAEA) and the World Meteorological Organization (WMO) since its initiation in 1961 (Rozanski et al., 1993). These data sets are helpful for portraying global and regional isotopic patterns (Bowen & Wilkinson, 2002; Rozanski et al., 1993), but the data suffers from coarse spatial and temporal resolution (Vuille, 2018). High frequency daily precipitation isotope sampling provides the opportunity to investigate further the relationship between meteorological parameters and isotopes, seasonality and the influence of moisture sources and trajectories on the isotopic values of precipitation.

In this study, a daily record of the isotopic composition of precipitation from Reykjavík, Iceland, from 30 June 2016 until 17 February 2020, is presented (hereafter IES isotope data). The more than 3 and a half years daily precipitation isotope data allows us to explore atmospheric processes that drive isotopic variability in the region.

The main objectives of this study are to: (1) document obtained daily isotopic values; (2) examine the impact of local weather on isotope variations; (3) examine seasonal and inter

annual variability of isotopic values; (4) compare the isotopic values of the IES precipitation samples to the isotopic values from ECHAM5-wiso general circulation model; (5) consider the possible influence of the North Atlantic Oscillation (NAO) on precipitation and isotope values; (6) construct an ISOTOPE database to be able to utilize the results from the measurements in this study as well as results from prior isotope measurements.

Research hypothesis

The water stable isotopic composition in an air mass is influenced by phase changes and fractionations. This for example means that every time moisture condenses in an air mass a "fingerprint" is left in the isotopic composition. I therefore hypothesize that there is a clear difference in the isotopic fingerprint of precipitation when studied in connection to different meteorological parameters, such as temperature, humidity, and precipitation amount.

Since the parameterization of the hydrological cycle is implemented in climate models, isotope-enabled climate models such as ECHAM5-wiso can capture the atmospheric isotope variations. By comparing the model with observations, I hypothesize that the isotopic record of daily precipitation samples will provide constraints on the assumption behind the parameterization of precipitation formation in the ECHAM5-wiso model.

Since the North Atlantic Oscillation (NAO) is influencing the atmospheric hydrological cycle, I hypothesize that the isotopic record of daily precipitation samples will improve the understanding of the variability of NAO.

1.1 The nature of Isotopes

Isotopes are any of two or more forms of a chemical element that have different numbers of neutrons but the same number of protons and electrons. The difference in the number of neutrons between the various isotopes of an element means that the various isotopes have different atomic weights (masses). Stable isotopes are chemical isotopes that are not radioactive and thus do not decay spontaneously with time (Kendall & Doctor, 2003). There are 275 isotopes of the 81 stable elements and there are over 800 radioactive isotopes (Thomas, 2013).

1.2 Stable isotopes of water (H_2O)

Water molecule is formed when one oxygen atom is covalently bonded with two hydrogen atoms. Both atoms have a range of isotopes that can be used as reliable tracers in environmental studies.

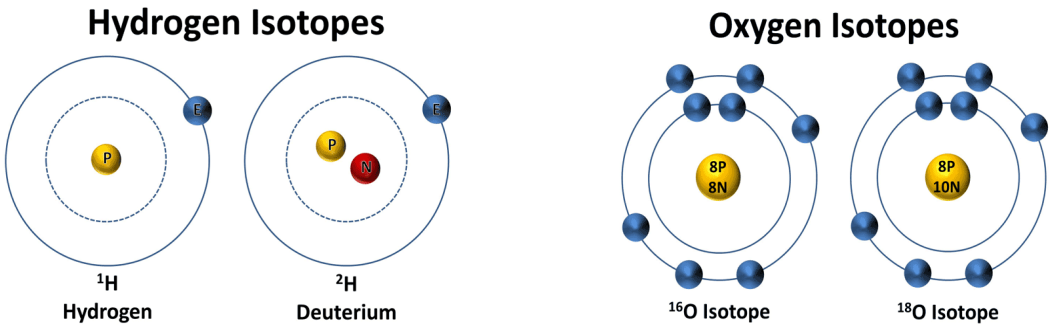

Figure 1.1 Isotopes of hydrogen and oxygen (NASA, 2016).

Hydrogen has 2 stable isotopes, Protium (regular Hydrogen) and Deuterium (Figure 1.1). Protium is the most abundant hydrogen isotope (99,98%) and its nucleus consists just from one proton. Deuterium (^{2}H or D) is the other stable isotope whose nucleus consists of both proton and neutron, and therefore has higher atomic mass than protium.

Oxygen has 3 stable isotopes (^{16}O, ^{17}O and ^{18}O) and 14 radioisotopes which half-life is a matter of seconds. ^{16}O is the most abundant isotope and composes 99,76% of total oxygen in the atmosphere, ^{18}O composes 0,2% and the other 0,24% is divided between oxygen radioisotopes and ^{17}O. ^{17}O is so rare that it is usually not accounted for when the water stable isotopes are used as tracers.

For hydrogen and oxygen the lighter isotopes are more abundant than the heavier ones Table 1.1.

Table 1.1 Abundance of stable hydrogen and oxygen isotopes (Gat, Mook, & Meijer, 2001).

Hydrogen	Abundance (%)	Oxygen	Abundance (%)
^{1}H	99.9850	^{16}O	99.759
^{2}H (D)	0.0155	^{17}O	0.037
		^{18}O	0.204

Isotopic composition is expressed as a ratio between the isotopic concentration of a sample to that of a known standard. This ratio is expressed in per mil (‰) and marked with the symbol δ. The isotopic composition of a sample is expressed by the following formula,

$$\delta = \left(\frac{R_{sample}}{R_{standard}} - 1\right) \times 1000\ ‰ \qquad (1.1)$$

where R is the isotopic ratio [$^{18}O/^{16}O$ or D/H] in a sample or standard (according to index) (Craig, 1961). If the δ value is positive, it means that sample has more of the heavy isotopes than the standard and is referred to as enriched (isotopically heavier) and if the δ value is negative then the sample has less of the heavy isotopes than the standard and is referred to as depleted (Clark & Fritz, 2013).

To be able to compare results from laboratories all over the world scientists have agreed to use a common standard. The Vienna Standard Mean Ocean Water (VSMOW) is commonly used for oxygen and hydrogen isotope standardization. Typically, δ values in the water cycle range from -450‰ to 100‰ and -50‰ to 50‰ for hydrogen and oxygen, respectively (Mook & Rozanski, 2000).

1.3 Isotopic fractionation

Only a small percentage of water (H_2O) molecules contain the heavier stable isotopes, ^{18}O and D (^{2}H, or deuterium), while the majority is composed of only ^{16}O and ^{1}H isotopes. Stable isotope ratios are highest in ocean water, intermediate in precipitation and lowest in water vapor and clouds. This is due to a process often referred to as isotopic fractionation, that occurs during the processes of evaporation and condensation. When water from oceans and lakes evaporates into the atmosphere, the water molecules composed of lighter isotopes evaporate more readily than those with heavier isotopes. As a result, atmospheric water vapor is isotopically lighter than ocean water. When water vapor then condenses to form precipitation, the heavier isotopes condense more readily than the lighter ones. This causes the $^{18}O/^{16}O$ and D/H ratios of precipitation to be less than that of ocean water, but greater than that of the water vapor (Figure 1.2) (Sharp, 2017).

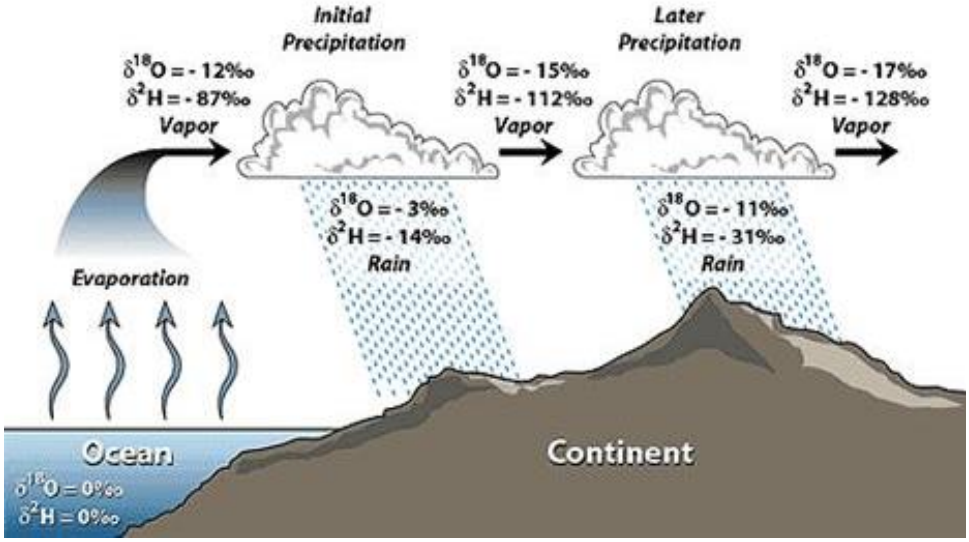

Figure 1.2 Schematic image of isotopic fractionation (Science, 2019).

1.4 Isotopic variations of precipitation

Geographic features, such as altitude and distance to big water bodies cause variations in the isotopic contents of precipitation. Seasonal temperature changes and precipitation amount are also important influential factors. The isotopic variations of precipitation can be summarized as follows:

Temperature / Seasonal effect: As water molecules with differing molecular mass have different vapor pressure, the lighter isotopes become enriched in the more volatile phase as

opposed to the less volatile phase. This effect, known as isotope fractionation (distillation), is strongly temperature dependent (Geyh, 2000). For instance, precipitation in winter is isotopically lighter than the precipitation in summer. This feature is more relevant in higher latitudes and less significant in lower latitudes.

Amount effect: It has been noticed that the $\delta^{18}O$ and δD values decrease with increasing amount of precipitation. Light/early rainfall tends to be enriched compared to heavy rainfall, in part due to evaporation of falling rain drops and partly due to decrease in temperature. This effect is more relevant in lower and middle latitudes and is less significant in regions with colder climates (Dansgaard, 1964).

The evaporation effect: Evaporation causes enrichment of the heavier isotopes in the liquid phase. Heavier molecules tend to have stronger bonds than the lighter ones. Hence, during evaporation, lighter molecules transit faster into gaseous phase. Isotopic characteristics of surface waters such as lakes and rivers, are often influenced by the evaporation effect (Dansgaard, 1964).

Inland effect: Heavier isotopes are preferentially removed from the clouds as precipitation, leaving the atmospheric water vapor more isotopically depleted (Figure 1.2). Accordingly precipitation becomes isotopically more depleted with increasing distance from the coast (Dansgaard, 1964).

Altitude effect: Isotopically lighter precipitation forms at higher altitudes where mean temperature is lower. Values of $\delta^{18}O$ decreases from -0.15 to -0.50‰ in 100 meters and δD values change between -1 and -4 ‰ accordingly (Dansgaard, 1964).

Latitude effect: With higher temperatures closer to the equator, precipitation is isotopically heavier than precipitation closer to the poles. This is caused by preferential removal of the heavier isotopes from clouds moving toward higher latitudes. In addition, the fractionation becomes stronger at higher latitudes due to lower temperatures (Dansgaard, 1964).

The above consideration of classical isotope effects illustrates the complexity inherent to the interpretation of stable isotopes in precipitation.

1.5 Meteoric Water Line (MWL)

The correlation between $\delta^{18}O$ and δD in long-term mean annual precipitation can be described by a linear relationship, expressed by (Craig, 1961):

$$\delta D = 8 \times \delta^{18}O + 10‰ \quad (1.2)$$

This regression line with a slope of 8 and an offset of 10‰ (Equation 1.2) is referred to as the Global Meteoric Water Line (GMWL) and underlines that $\delta^{18}O$ and δD generally are

subject to the same atmospheric processes, but the δD fractionation is 8 times stronger than that of $\delta^{18}O$. The 10‰ offset, is due to kinetic fractionation effects (Craig, 1961).

The mean seasonal cycle of stable isotope composition at a station generally varies along the GMWL. For some stations, significant deviations from the GMWL have been noticed, and for this reason Local Meteoric Water Lines (LMWL) have been established. This is due to local processes, such as rainwater evaporation and seasonal transport changes rather than different fractionation processes, hence using LMWL can be a misleading concept (Gat 1996). For Iceland, 2 different water lines have been identified using results of mean annual groundwater samples from different parts of Iceland. One expresses the relationship for precipitation with $\delta^{18}O$ values higher or equal to -10.5‰ (Eq. 1.3) and other expresses the relationship for precipitation with $\delta^{18}O$ values lower or equal to -10.5‰ (Eq. 1.4) (Sveinbjörnsdóttir, Johnsen, & Arnórsson, 1995).

$$\boldsymbol{\delta D} = \begin{cases} \mathbf{6.55} \times \boldsymbol{\delta^{18}O} - \mathbf{3.5}‰ & \textbf{if } \boldsymbol{\delta^{18}O} > -\mathbf{10.5}‰ \\ \mathbf{8} \times \boldsymbol{\delta^{18}O} + \mathbf{11}‰ & \textbf{if } \boldsymbol{\delta^{18}O} \leq -\mathbf{10.5}‰ \end{cases} \quad (1.3)\ (1.4)$$

1.6 Deuterium excess (*d*-excess)

Information on the origin of precipitation and physical conditions at the site of formation can be interpreted using deuterium excess (hereafter *d*-excess) defined as:

$$\boldsymbol{d = \delta D - 8 \times \delta^{18}O} \quad (1.5)$$

According to Dansgaard (1964), the deuterium molecule is much less sensitive to kinetic effects than ^{18}O. This means that the $H_2{}^{16}O$ and $H_2{}^{18}O$ react more readily than $HD^{16}O$ (Dansgaard, 1964). Under equilibrium conditions the difference in diffusivity of the isotopes results in a slope of 8 (Eq. 1.2). D-excess can be visually depicted as an index of deviation from the Global Meteoric Water Line (GMWL) and be used as an indicator of non-equilibrium processes. It is a useful parameter because it is correlated with the physical conditions, mainly the relative humidity, and to a lesser extent, air- and sea surface temperature (SST) and wind speed at the vapor source regions (Froehlich, Gibson, & Aggarwal, 2002). An increase in relative humidity leads to lower *d*-excess while increase in SST results in higher *d*-excess (Merlivat & Jouzel, 1979; Stephan Pfahl & Sodemann, 2014).

Past studies show that the isotope content in precipitation depends on the history of the precipitating air masses. The *d*-excess factor is considered a good indicator of the origin of water vapor or the source of precipitation (Johnsen, Dansgaard, & White, 1989). Despite these advantages, the use of *d*-excess still has some drawbacks. Compared with the application of the individual isotopes of $\delta^{18}O$ or δD, *d*-excess variations can be complicated, and theoretical understanding of *d*-excess and related climatic controls has not yet been fully explored (Froehlich et al., 2002).

1.7 General Circulation Models (GCMs)

General circulation models (GCMs) are used in weather forecasting. They are highly detailed grid-based simulations of weather and use atmospheric physics to predict events over hours, days and even to predict climate change over years, decades, or centuries. With better understanding of the physics of the atmosphere, GCMs have become more and more accurate. This has helped scientists to gain substantial new insights into our present and past climate.

In recent years, there have been several significant advances in water isotopes modelling in GCMs. In addition to development of the models, validation with real-world data is of paramount importance. This is to ensure that what is being simulated are real physical phenomena in nature. Only after GCMs have been validated with global measurements of water isotopes can they be deployed with confidence to address scientific questions such as changes in the global precipitation patterns and large-scale atmospheric circulations (Xi, 2014).

1.7.1 The ECHAM5-wiso General Circulation Model

ECHAM5 is a general circulation model (GCM), developed by the Max Planck Institute for Meteorology, in Hamburg, Germany. The model has been developed from the ECMWF operational forecast model cycle 36 (1989) (hence the first part of its name, EC) and a comprehensive parameterization package that has been developed at the institute in Hamburg (hence the abbreviation HAM). A comprehensive model description of ECHAM5 is given by (Roeckner et al., 2003). Stable water isotope module has been implemented into the atmospheric ECHAM5 model, referred to as EHCAM5-wiso (Werner, Langebroek, Carlsen, Herold, & Lohmann, 2011). The ECHAM5-wiso simulation results are in good agreement with available observations of the isotopic composition of precipitation from the Global Network of Isotopes in Precipitation (GNIP), on both seasonal and annual scale (Werner et al., 2011). However, as the model is predicting isotopic composition of the atmospheric water vapor and precipitation in much higher frequency it is more relevant to compare the simulations to a daily sampled precipitation. In this study the ECHAM5-wiso simulation was compared to the observation of the isotopic composition from the IES isotope dataset and available meteorological data.

1.8 The Icelandic Low and the North Atlantic Oscillation (NAO)

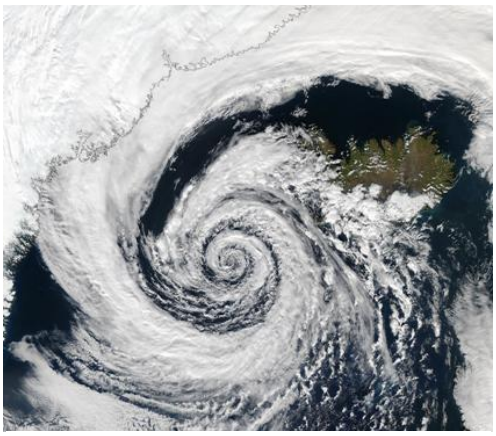

Figure 1.3 Deep low-pressure area off Iceland, September 2003 (NASA, 2019).

The Icelandic Low is a term used for describing the semi-permanent low-pressure center near Iceland (mainly between Iceland and southern Greenland) on mean charts of sea-level pressure and is a principal center of action in the atmosphere circulation of the Northern hemisphere (Figure 1.3). As this semi-permanent low-pressure system intensifies and weakens, it affects the amount of air (generally warm) being brought into the Arctic to the east of the low and the amount of air (generally cold) being swept out of the Arctic to the west. The Icelandic Low is part of a larger weather pattern called the North Atlantic Oscillation (NAO). NAO is the name for changes in the difference of air pressure between the Icelandic Low and a semi-permanent high-pressure system centered near the Azores Islands. Both systems are present all year but are strongest in winter. When both the high and the low intensify and fluctuate in pressure relative to one another, they change the circulation of cold and warm air in the region. NAO is usually defined through changes in the surface pressure, into positive or negative phase and dictates climate variability from the eastern part of North America to Siberia and from the Arctic to the subtropical Atlantic, especially during winter (Visbeck, Hurrell, Polvani, & Cullen, 2001).

NAO is in a positive phase when both the subpolar low and the subtropical high-pressure center is stronger than the average. The increased difference in pressure between the two regions results in a stronger Atlantic jet stream and the storm track shifting northwards. Consequently, northern Europe experiences increasing number of storms with more precipitation and temperatures warmer than average, due to air masses arriving from lower latitudes. At the same time, southern Europe experiences fewer storms and precipitation below average. In eastern North America, the positive phase of the NAO generally brings higher air pressure, with mild and wet winter conditions, while Canada and Greenland experience cold and dry winters.NAO is in a negative phase when both the subpolar low and the subtropical high-pressure centers are weaker than average. The reduced pressure gradient results in fewer and weaker winter storms crossing on a more west-to-east pathway, with precipitation below average and temperatures lower than average in northern Europe. Conversely, southern Europe experiences increased number of storms, with precipitation above average, and temperatures that are warmer than average. In eastern North America, the negative phase of NAO generally brings lower air pressure, with stronger cold-air outbreaks and snowy weather conditions. Greenland, however, will have milder winter temperatures (Visbeck et al., 2001).

A record of NAO phases from 1950 through the present is available from NOAA's Climate Prediction Center. This data is used in this study for comparison with measured IES and IMO isotope data.

2 Geographical and climate setting of the study area

Although Iceland is located close to the Arctic circle, it enjoys a much milder climate than both its name and location would imply. A branch of the Gulf Stream flows along the southern and the western coast and moderates the climate greatly. This brings mild Atlantic air in contact with colder Arctic air which results in a climate that both has frequent changes in weather (Figure 2.1).

Figure 2.1 Geographical setting of the study area. Source: NOAA (left) and Landmælingar Íslands (right).

Furthermore, this leads to more rainfall in the southern and western part of the country than in the northern part (Einarsson, 1984). Monthly averages for the 30-year period from 1961-1990, for precipitation and temperature in Reykjavík, are plotted in Figure 2.2.

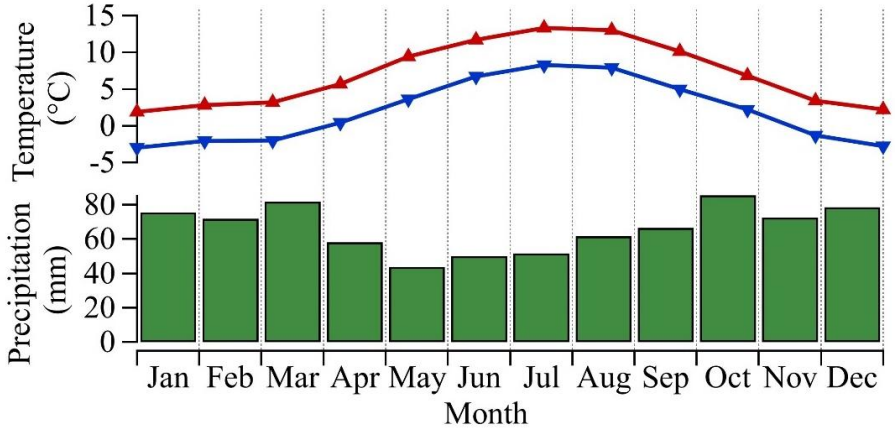

Figure 2.2 Monthly averages (1961-1990) for temperature and precipitation in Reykjavík. Red line represents the mean daily maximum temperature (°C) and blue line represents the mean daily minimum temperature (°C). Green columns represent the mean total precipitation (mm). Source: (World Meteorological Organization, 2020).

2.1 Meteorological data and statistical methods

Meteorological data was used for interpretation of the results of isotopic measurements of daily precipitation samples. The meteorological data obtained from the Icelandic Meteorological Office (hereafter IMO) includes temperature (°C), relative humidity (%), pressure (hPa), and precipitation amount (mm).

The distance between the sample site in Vatnsmýri and IMO, is approximately 2.2 km in straight line (Figure 3.1). There are 2 weather stations located at IMO in Reykjavík. Station number 1 is a manned synoptic station (64°07.648' N, 21°54.166' E) at 52 meters above sea level (a.s.l.) and station number 1475 is an automated observational station (64°07.653' N, 21°54.120' E) at 52 meters a.s.l. Daily average temperature (°C), precipitation amount (mm), relative humidity (%) and pressure hPa) were obtained from station 1. For the more frequent sampling from a low-pressure event on 18 September 2019, 10 minute' data was obtained from station 1475.

Specific humidity was calculated using temperature, pressure and relative humidity data from IMO, using bigleaf package in R language (Knauer, El-Madany, Zaehle, & Migliavacca, 2018). Specific humidity is sometimes referred to as the humidity ratio and shows the ratio of the amount of water vapor in the air to the amount of dry air in the area. Meteorological data was used to link precipitation isotopes with weather conditions at the sampling site.

To summarize the strength of this relationship, standard statistical techniques such as linear regression was used. Pearson's correlation coefficient was used to measure the strength of the linear association or correlation, denoted by r. This method is based on the method of covariance and gives information about the strength of correlation as well as the direction of the relationship. Correlation is considered strong if $|r| \geq 0.5$ but weak if $|r| < 0.5$. P-values were calculated to determine if the association was statistically significant or not, with $p < .05$ being statistically significant and $p < .001$ being statistically highly significant. All statistical analyses were performed using the R language (Team, 2013). Same statistical methods were used for comparison of measured isotope and meteorological data to the ECHAM5-wiso general circulation model and the NAO index.

3 Methods

3.1 Sample collection

3.1.1 Daily sampling of precipitation

Precipitation was sampled from a collector installed in Vatnsmýri in Reykjavík, Iceland, close to Askja, the building of Natural Sciences at the University of Iceland (64°08.14'N, -21°56.45'E), at 16 meters a.s.l. The collector was made of a funnel connected to a 500 mL plastic container from Cole-Parmer. A spout at the bottom of the container allowed an easy sample collection. The funnel at the top was featured with a sieve on top to prevent dirt entering the samples (Figure 3.1). A layer of paraffin oil floating on top of the rainwater inside the container prevented evaporation inside the container and mixing with surrounding atmospheric moisture. Even though the sample collector is placed in plain sight and not far from a walking path it was left untouched most of the sampling period, only once it was vandalized and had to be replaced. Some samples were collected into 60 mL gas-tight amber glass bottles while others were collected in plastic bottles. The plastic bottles were stored in the freezer before measuring while the amber glass bottles were stored in a fridge.

Figure 3.1 Sampling site and location of IMO (left) and the sample collector (right) . Aerial photograph (Já, 2020).

The collection of daily precipitation started on 30 August 2016 and is still ongoing. In this study the last sample considered was collected on 17 February 2020. Thus, the dataset studied here covers daily precipitation samples, more or less continuous, for 3 and a half years. After a heavy rain, sometimes more than one sample was collected from the sample container. In most cases, the difference between two duplicate measurements was not significant, (less or equal to 0.1‰ and 1‰ for $\delta^{18}O$ and δD respectively) and in those cases

the average was taken between the two results and used as the final isotopic value. After filtering out the duplicate measurement, the isotopic value was determined for a total of 344 samples.

There are gaps in the daily precipitation record mainly due to no rain, e.g. the exceptionally dry period in Reykjavík in June 2019 (Figure 3.2) and some are due to lack of sampling during holiday seasons. There is a gap in the data sampling from April 25th - May 28th 2018 but the longest gap is from January 11th - March 19th 2019 when the water in the plastic sample container froze, resulting in it to crack. Unfortunately there was over a month's delay in getting a replacement and during that time no collection took place.

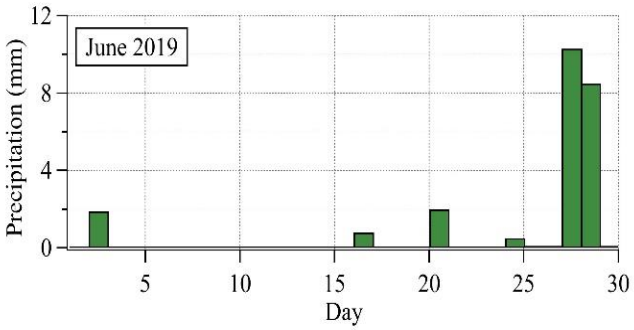

Figure 3.2 Precipitation in Reykjavík in June 2019 (Veðurstofa Íslands, 2019e).

3.1.2 Sampling on 18 September 2019

The weather forecast for 18 September 2019 with the prospect of heavy rain, presented a good opportunity for a more frequent sampling of precipitation (Figure 3.3). Combined infrared thermal satellite image with reflections from a weather radar in Iceland shows the precipitation over Reykjavík at 08:00 in the morning of September 18th (Figure 3.3).

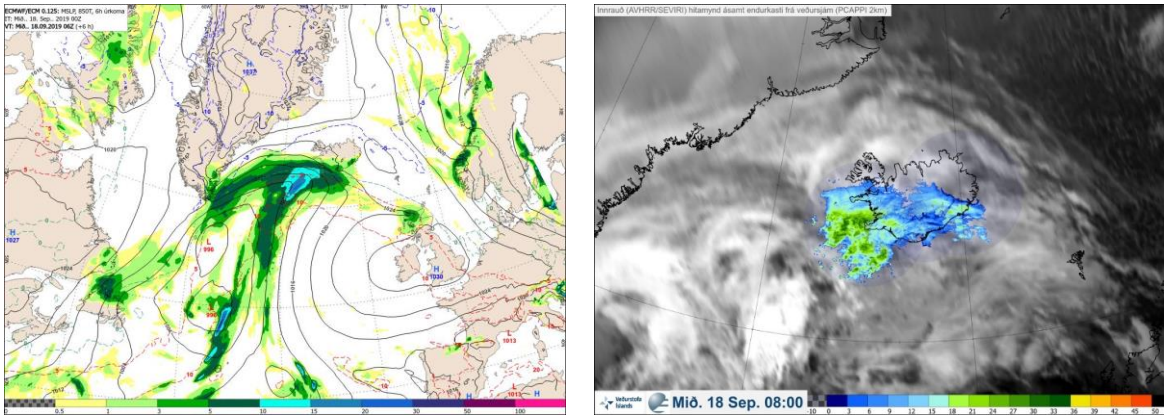

Figure 3.3 Weather forecast for September 18th 2019 at 06:00 (left). Combined infrared (AVHRR/SEVIR) thermal satellite image with reflection from weather radar in Iceland, from September 18th 2019 at 08:00 (right) (Veðurstofa Íslands, 2019a, 2019c).

In the morning of September 18th, at 8:30 the sampler was emptied of the last 24-hour precipitation and after that samples were collected at 30 minute' interval. The last sample was collected at 14:30 (at 15:00 there was no precipitation in the collector). This front went over the sampling site a little faster than the forecast had predicted but still gave 12 valuable samples. All the samples were put into 60 mL airtight amber glass bottles and stored in a fridge until measured.

3.2 Stable isotope measurements

The isotopic composition of the collected precipitation samples was measured using a Cavity Ring-Down Spectrometer, L2130-*i* (Picarro Inc., USA) and a Delta V Advantage Isotope Ratio Mass Spectrometer (IRMS) from Thermo Scientific, both located at the Institute of Earth Sciences, University of Iceland (IES) (Figure 3.4). The advantage of using the Picarro is that is measures both $\delta^{18}O$ and δD values simultaneously with similar precision as the IRMS, where each isotope is measured separately with different preparation methods. The largest part of the precipitation samples was measured using the Picarro but the IRMS was used while the Picarro analyzer was away for repair. Same samples were also measured with both equipment to establish measurement precision.

Figure 3.4 The Picarro L2130-I (left) and the Delta V Advantage IRMS (right).

3.2.1 The Picarro laser isotope analyzer

The Picarro laser isotope analyzer uses a sensitive optical spectroscopic technique to determine δD and $\delta^{18}O$ ratios. The instrument consists of high precision Vaporizer and an auto-sampler connected to an Analyzer. Two vacuum pumps secure stable pressure. The sample is injected into the Vaporizer using a 5µL syringe placed in the auto-sampler. The sample is directed into the analyzer after it has been evaporated. A special analyzing technique that is utilized and developed by Picarro is referred to as Cavity-Ring-Down Spectroscopy (CRDS).

It consists of a laser with three reflective mirrors for illumination of optical cavity. When the laser is on, the cavity fills with circulating laser light and due to constructive interface intensity builds up. Afterwards, gas spaces which absorb the light, are introduced to the cavity. The decaying light leaks off from the cavity after the laser is switched off. Meanwhile, light is reflected between mirrors numerous times. Hence, Picarro measures how long it takes for a light to decay to 1/e of its initial intensity and this "ringdown time" is then used to calculate the concentration of light absorbing substance in the cavity (Figure 3.5) (Picarro, 2019).

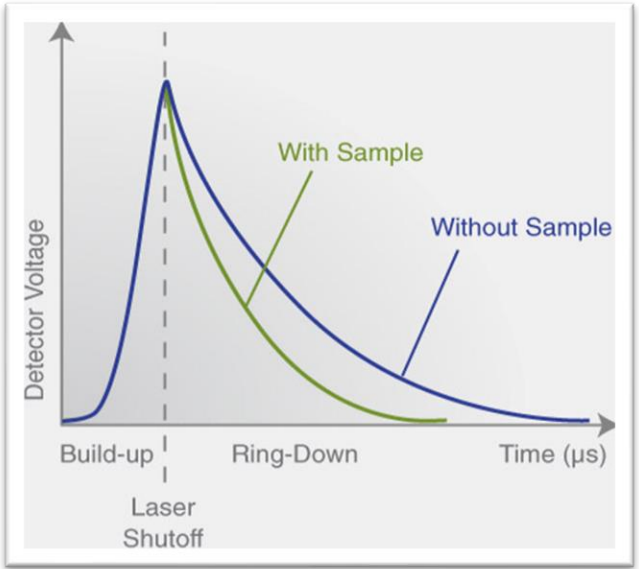

Figure 3.5 The difference between the ringdown timing with and without a sample (Picarro, 2019).

For the Picarro measurements, water samples and working standards were put into 0.5 mL vials and sealed with caps with septa. The samples were then placed in a sample tray connected to an auto-sampler for measurement (Figure 3.4).

3.2.2 Isotope Ratio Mass Spectrometry (IRMS)

In the Isotope Ratio Mass Spectrometry (IRMS) instrument, ions are accelerated to a high speed in an electric field and then shot into a magnetic field, which applies a force perpendicular to the ions' direction of travel. An ion source, located in the ion chamber, ionizes the sample gas. The force from the magnetic field deflects ions to different degrees, depending on their mass-to-charge ratio. Lighter ions are deflected more than heavier ones, so when they reach the detector at the other end of the mass spectrometer, it measures the deflection of each ion beam. A current generating metal structure, a Faraday collector (cup) then collects the appropriate ions (Fig. 3.6). This measurement can then be used to calculate the mass-to-charge ratio of the ions, which allows the chemical and isotopic composition of the sample to be determined. A computer software calibrates the isotopic ratio of the reference gas by comparing it to a known standard, which also eliminates any instrumental errors. For stable water isotopes, the Vienna Standard Mean Ocean water

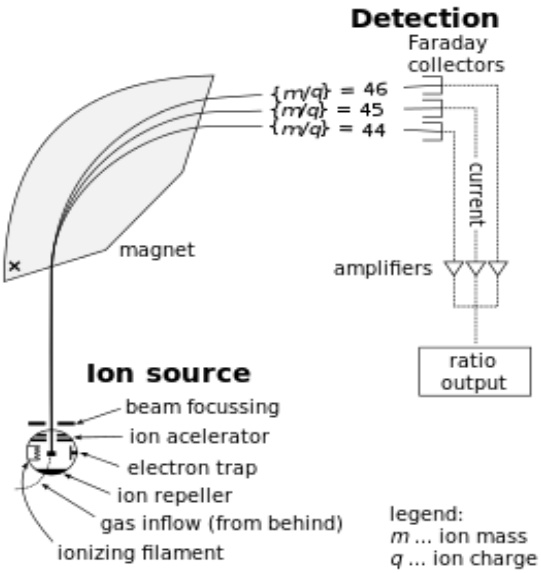

Figure 3.6 Schematics of a simple mass spectrometer with sector type mass analyzer measuring CO_2 (U.S. Geological Survey, 2013).

(VSMOW) standard is used. Sample can be injected into the IRMS via different inlets. The inlet that is used at the Institute of Earth Sciences is a Gas Bench II device.

3.2.3 Gas Bench II

The conversion of any type of organic or inorganic compound into simple gases is the basic principle for IRMS. The water samples were analyzed using the Gas Bench II device together with Isotope Ratio Mass Spectrometer (IRMS) Delta V Advantage. The Gas Bench II is a flexible continuous flow preparation device and inlet system with repetitive loop injection of gases, controlled by an auto-sampler from CTC Analytics, GC PAL (Figure 3.7). When measuring samples in IRMS with Gas Bench II, 200 µL of sample water is placed into 12 mL exetainers (Labco Limited, UK). The vials are then sealed with septa and all air removed from the sample vials by an automated, auto-sampler assisted flushing procedure using a mixture of either H_2 (for δD) or CO_2 (for $\delta^{18}O$) in He. The H_2 or CO_2 in the flushing He stream is used as equilibration gas. The equilibration time in 21°C regulated sample tray, is minimum 24 hours for $\delta^{18}O$ and minimum 1 hour for δD, using a platinum catalyst in the δD measurements. After required equilibration time, the gas mixture gets transported from the vials into a water trap before entering the valco valve (Figure 3.8). A valco valve controls the sample volume, or pulses, that go into the GC column. Another water trap awaits the sample gas when it exits the GC and enters the open split where it is finally injected into the IRMS (Thermo-Fisher, 2019).

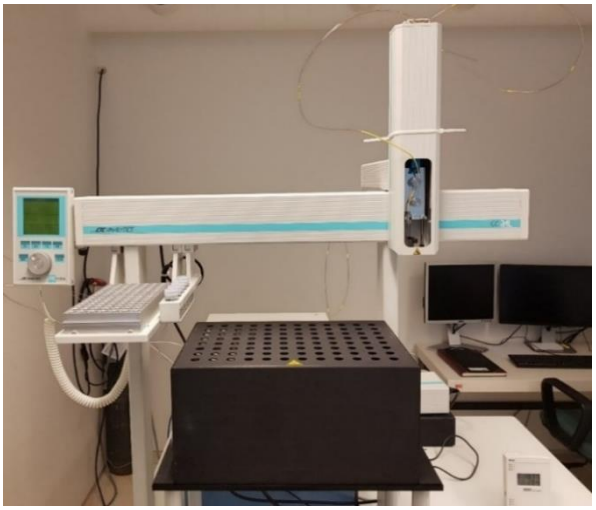

Figure 3.7 GC PAL auto-sampler used with Gas Bench II(Photo: Rósa Ólafsdóttir).

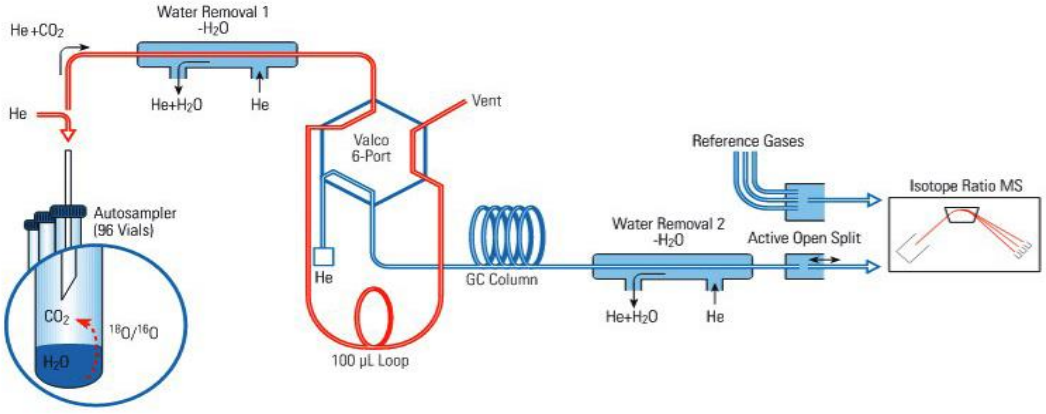

Figure 3.8 Schematic diagram of the sample path in Gas Bench II (Thermo-Fisher, 2019).

3.3 Calibration and precision

Results from the isotope analyzers are reported as δ-values. To define δD and $\delta^{18}O$ ratios in the samples, 3 working standards of known isotopic composition were used in the analysis (Table 3.1).

Table 3.1 Isotopic composition of working standards.

Standard	**$\delta^{18}O$ (‰)**	**δD (‰)**	
Bermuda-0	0.53	6.26	High values
NEEM (Greenland)	-33.52	-257.11	Low values
GV (Gvendarbrunnar)	-8.54	-57.72	Values close to measured samples

Part of the IRMS measuring procedure is the linearity test using a reference gas, also referred to as an On Off test. It measures how linear the values of ten peaks are. A different reference gas is used depending on which isotopes are to be measured. The standard deviation (SD) of those ten peaks is then calculated. A SD below 1.0 for δD and below 0.1 for $\delta^{18}O$ is acceptable, the same as with the measurement precision.

The accuracy of the calculated sample values depend on the accuracy of the working standards measured in each run. The difference between the known value and the measured value is calculated to estimate the accuracy of the whole run. If the residual is below 0.1‰ for $\delta^{18}O$ and 1.0‰ for δD, the run is considered to show satisfying results.
A memory effect from the sample measured before can be seen when measuring isotopes with the Picarro analyzer. To eliminate the memory effect as much as possible, parts of the measurements were removed when estimating the average value for each sample. The working standards were analyzed 25 times each with the first 20 times removed and for the precipitation samples, the first 6 of 10 were removed. The rest was then used in the data analysis. The programming language Matlab was used for calculations and corrections for memory effects using a script prepared by Steen-Larsen (2018). Memory effect is not a problem when using the IRMS with Gas Bench II, where each sample or standard injected is measured 10 times and the first and last peaks are removed before calculation of the average δ-value of the remaining 8 peaks. For both measurement methods, working standards were placed in between samples to make sure that there was no drift within each measurement.

3.3.1 IAEA Water Isotope Inter - Comparison (WICO2016)

The Institute of Earth Sciences (IES) took part in an evaluation of 235 international laboratories conducting water isotope analysis by isotope-ratio and laser-absorption spectrometry organized by the International Atomic Energy Agency (IAEA) in 2016 (Wassenaar et al., 2018). In this IAEA Water Isotope Inter-Comparison test (WICO2016) water samples were distributed to the laboratories, consisting of samples spanning the common δ-range of natural waters. Those samples were measured in the IES lab, using the Picarro L2130-i, during summer of 2016 and the results sent to IAEA.
The standard deviation for proficiency assessment (SDPA) is the maximum acceptable difference between the assigned delta value and the laboratory submitted delta value result. The SDPA was set to 0.2‰ for $\delta^{18}O$ and 1.5‰ for δD (Wassenaar et al., 2018). Point

Scoring was used to further convey overall laboratory performance, where combined point score of 12-10 rated excellent, 9-7 points acceptable, 6-4 points questionable and 3-0 points unacceptable. The results for both $\delta^{18}O$ and δD measurements in the IES laboratory got rated as excellent, the results for $\delta^{18}O$ presented in **Error! Reference source not found.**. More detailed results are found in the research article published by Wassenaar et al. (2018).

1.1 Oxygen-18 ($\delta^{18}O$)

Laboratory token: 16199

Instrument 1: Laser spectrometer (LPicarro2031-i)

Sample	Reported values $\delta^{18}O$	d-excess	Assigned values $\delta^{18}O$	d-excess	Outlier	Bias	Score Points	z Score	
WICO 1	-10.80 ± 0.05	8.7	-10.80 ± 0.02	9.0		0.00	3	0.00	acceptable
WICO 2	-5.11 ± 0.05	-1.3	-5.11 ± 0.03	-0.8		0.00	3	0.00	acceptable
WICO 3	-22.06 ± 0.05	7.3	-22.01 ± 0.05	7.8		-0.05	3	0.25	acceptable
WICO 4	-0.51 ± 0.05	4.3	-0.50 ± 0.05	4.5		-0.01	3	0.05	acceptable

Total Score Points WICO 2016: 12 (Excellent)

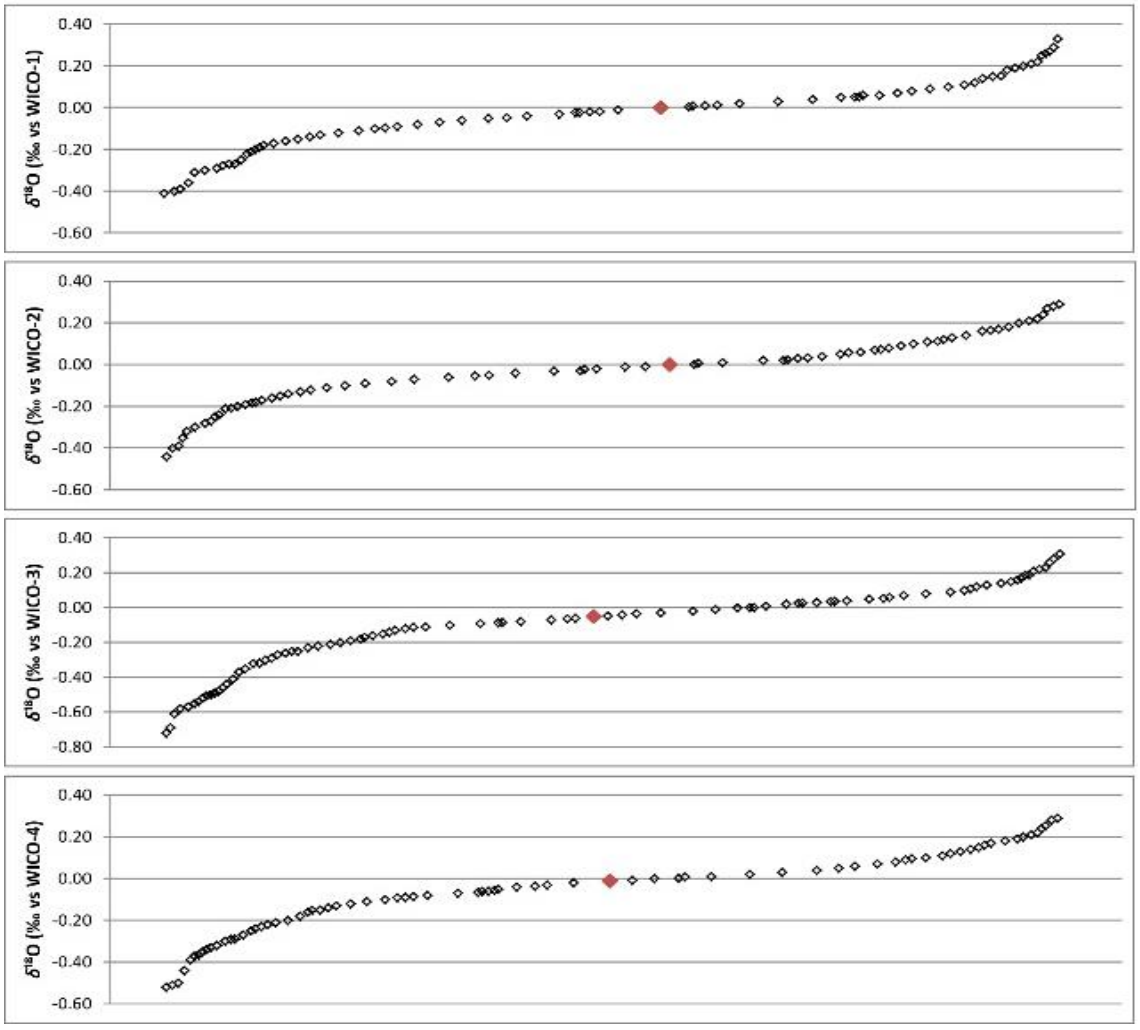

Figure 3.9 Results for IES laboratory $\delta^{18}O$ isotope measurements (red diamonds) in comparison to other participants in WICO2016.

4 Institute of Earth Sciences (IES) - ISOTOPE database

A part of this study was to compile a database for all the isotopic measurements that have been carried out at the Institute of Earth Sciences (IES) since the arrival of the Mass Spectrometer in the year 2006. The structure of the database is listed in Table 4.1.

Table 4.1 Structure of the IES – ISOTOPE database.

Data field	Description	Format (units)
Run	Number of Run	Text
Date	Date of measuring	Date (YYYY:MM:DD)
Time	Time of measuring	Time (hh:mm)
Tray number	Position of sample in measuring trays	Number
Client	Who ordered the measurements	Text
Sample	Sample number	Text
Sample_extra_info	Extra information about the sample	Text
Time_of_sampling	If the information is available, at what time was the sample collected?	Time (hh:mm)
Method	Different methods for measurements, Gasbench II, Picarro or TC/EA	Text
d_18O/16O(average)	Average of the raw data (of 10 or 8 samples) - $\delta^{18}O$	Number
d_18O/16O(stdev)	Standard deviation for 10 or 8 measurements of the same sample - $\delta^{18}O$	Number
δsample_18O/16O	Calculated final value for $\delta^{18}O$	Number
d_3H2/2H2(average)	Average of the raw data (of 10 or 8 samples) - δD	Number
d_3H2/2H2(stdev)	Standard deviation for 10 or 8 measurements of the same sample - δD	Number
δsample 3H2/2H2	Calculated final value for δD	Number
Project_number	Project number where available	Text
Arrival_date	The date when the samples arrived at the lab at the Institute of Earth Sciences, UI	Date (YYYY:MM:DD)
Storage_method	How the samples are stored (fridge, freezer, or table)	Text
Bottle_type	Type of bottle, glass, or plastic	Text
Remarks	Extra remarks about the sample if needed	Text

Databases are important components for scientific research. They ensure the longevity of data and enable further investigation of scientific ideas. Modern databases also serve as digital libraries for research and if well-organized they allow users to find, visualize and analyze a great amount of data using search and analysis tools. The usefulness of any database is limited by both the quantity (the statistical significance) and quality of the data. Extra information about the samples or metadata, is important to provide context for the isotope data and help with interpretation. Geographic locations, dates of sampling, measuring methods as well as methods of storing can all affect the outcome and are thus important information in the database.

The database is an ongoing project but at the time this is written the total number of entries in the database are up to more than 46.000.

5 Results

In this chapter, the analytical results of the first comprehensive daily precipitation isotope data ($\delta^{18}O$, δD and calculated *d*-excess) in Iceland are presented (Figures 5.1 - 5.3 and Table 5.1). The full dataset with meteorological data from IMO is given in Appendix A.

5.1 The IES isotope data

The total dataset from the IES isotope observations consists of 344 samples from the period from 30 June 2016 until 17 February 2020.

Mean values for daily observations with their associated standard deviation (SD) and minimum and maximum values are listed in Table 5.1. The isotopic daily mean of $\delta^{18}O$ and δD vary between -17.48‰ and -0.67‰ for $\delta^{18}O$, and between -132.3‰ and 1.3‰ for δD. The *d*-excess values vary between -7.5‰ and 31.4‰ (Table 5.1).

Table 5.1 Mean values and associated standard deviations, minimum and maximum values of the observed IES isotopic data ($\delta^{18}O$, δD and d-excess) and meteorological data from IMO (temperature, specific humidity and precipitation amount).

	IES / IMO data	**Min.**	**Max.**
$\delta^{18}O$ (‰)	-8.55 ± 3.1	-17.48	-0.67
δD (‰)	-61.1 ± 25.7	-132.3	1.3
d-excess (‰)	7.4 ± 6.6	-7.5	31.4
Temperature (°C)	5.9 ± 4.6	-6.4	16.1
Specific humidity (g/kg)	4.6 ± 1.5	1.3	8.9
Precipitation (mm)	4.6 ± 5.3	0.0	34.8

In Figure 5.1, the results from the measurements of the IES isotope data, $\delta^{18}O$, δD and calculated *d*-excess, are plotted on a timeline together with the meteorological data obtained from IMO, precipitation amount, temperature and calculated specific humidity. The data from IMO is continuous while the isotopic data is only displayed for the observation days, explaining the visible gaps in the isotopic data for $\delta^{18}O$, δD and *d*-excess (Figure 5.1).

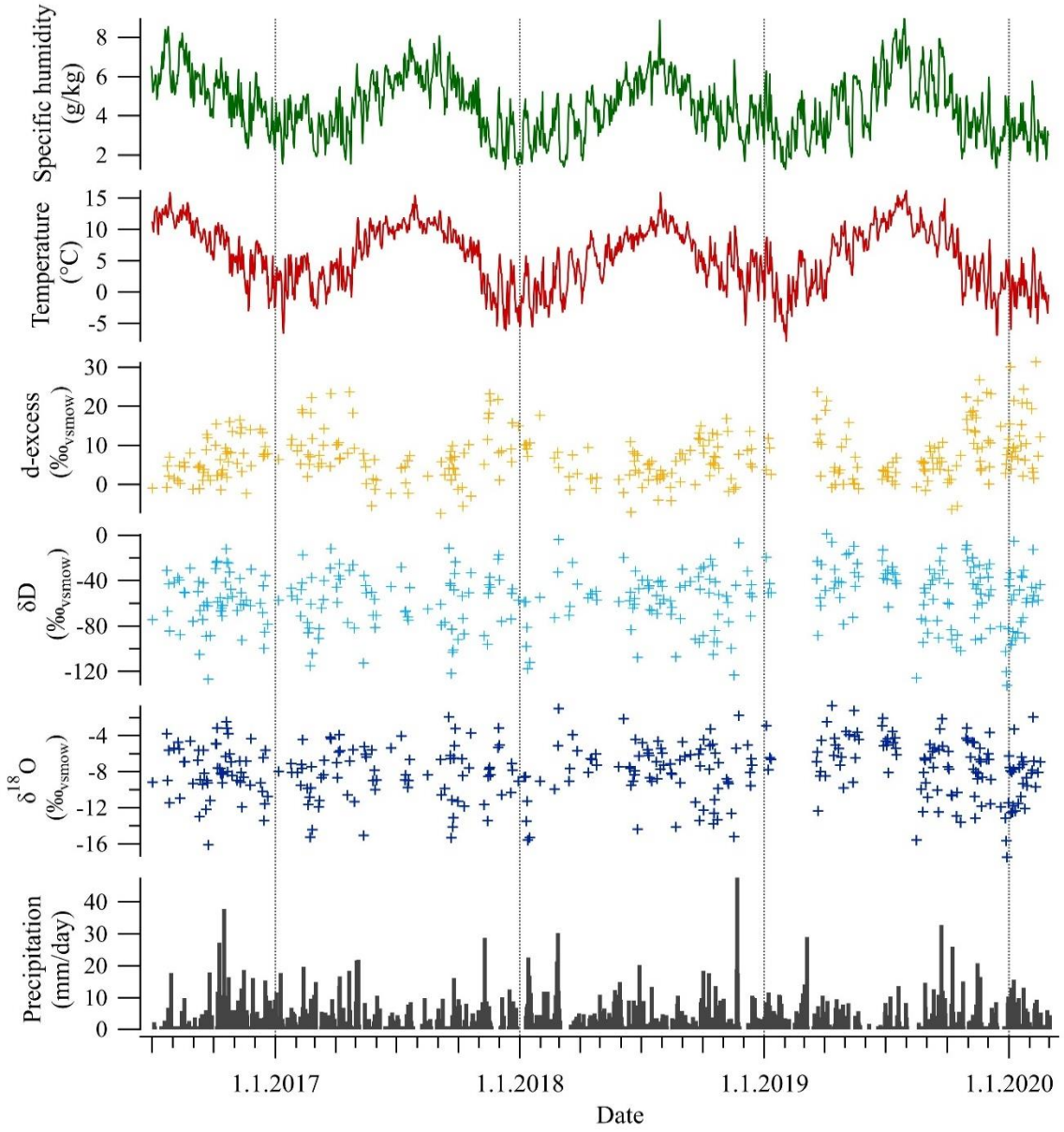

Figure 5.1 Results for $\delta^{18}O$, δD and d-excess plotted against meteorological data from IMO (precipitation, temperature and specific humidity).

The first thing that is noticed is that the IES isotope data exhibits seasonality. The values for *d*-excess are higher in winter and lower in the summer, while the $\delta^{18}O$ and δD data show the opposite trend, i.e. lower values during winter and higher values in the summer. Calculated linear regression results between the isotopic and meteorological data are listed in Table 5.2. There is a strong significant anti-correlation between *d*-excess and temperature (r = -0.61 ± 0.05) and between *d*-excess and specific humidity (r = -0.56 ± 0.05), while the $\delta^{18}O$ values do not show as strong correlation with temperature and specific humidity, with r values of only 0.26 ± 0.05 and 0.22 ± 0.05, respectively (Table 5.2). A weak anti-correlation is seen between the $\delta^{18}O$ values and the precipitation amount (r = -0.19 ± 0.05) but no correlation is observed between precipitation amount and *d*-excess (r = 0.03 ± 0.05) (Table 5.2). The relationship between specific humidity and temperature is strong (r = 0.88 ± 0.03) (Table 5.2) as observed in Figure 5.1.

Table 5.2 Linear regression results (slope and correlation coefficients – r and p-values) for observed IES isotope data and IMO meteorological data.

Slope IES / IMO data	**Total data***	***P* - value**
$\delta^{18}O$ vs. temperature	-9.17 ± 0.31	
	r = 0.26 ± 0.05	$p < .001$
$\delta^{18}O$ vs. specific humidity	-10.39 ± 0.63	
	r = 0.22 ± 0.05	$p < .001$
$\delta^{18}O$ vs. precipitation	-7.36 ±0.22	
	r = -0.19 ± 0.05	$p < .001$
d-excess vs. temperature	13.72 ± 0.04	
	r = -0.61 ± 0.05	$p < .001$
d-excess vs. specific humidity	20.69 ± 1.13	
	r = -0.56 ± 0.05	$p < .001$
d-excess vs. precipitation	7.0 ± 0.5	
	r = 0.03 ± 0.05	$p = .626$
Specific humidity vs. temperature	3.05 ± 0.07	
	r = 0.88 ± 0.03	$p < .001$

* 344 observation days. The uncertainty on the slope represents the standard deviation and the uncertainty on the correlation coefficient represents the standard error.

The distribution of isotopic and meteorological data is presented in histograms in Figure 5.2. The distribution for $\delta^{18}O$, δD temperature and specific humidity (Figure 5.2, a,b and e) is approximately Gaussian, which is not the case for the *d*-excess and precipitation (Figure 5.2, c and f).

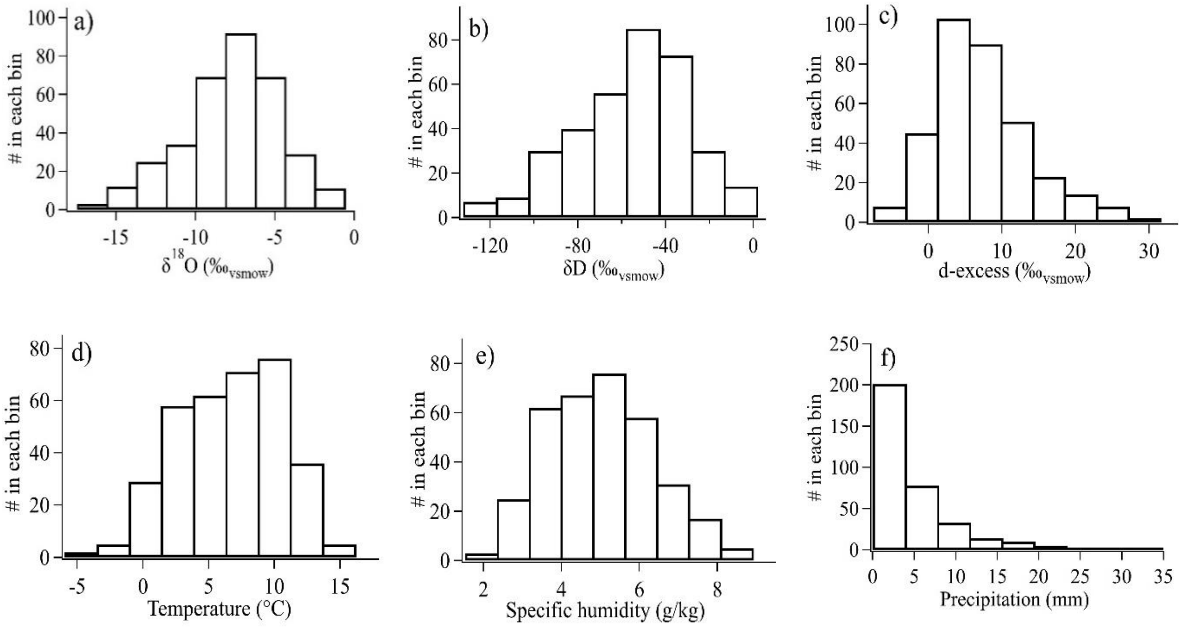

Figure 5.2 Distributions of $\delta^{18}O$ (a), δD (b) and d-excess (c), temperature (d), specific humidity (e) and precipitation (f) for IES isotope data and meteorological variables (IMO).

The linear relationship of the isotopic values in the measured IES precipitation samples is displayed in Figure 5.3, where $\delta^{18}O$ values are plotted against δD values.

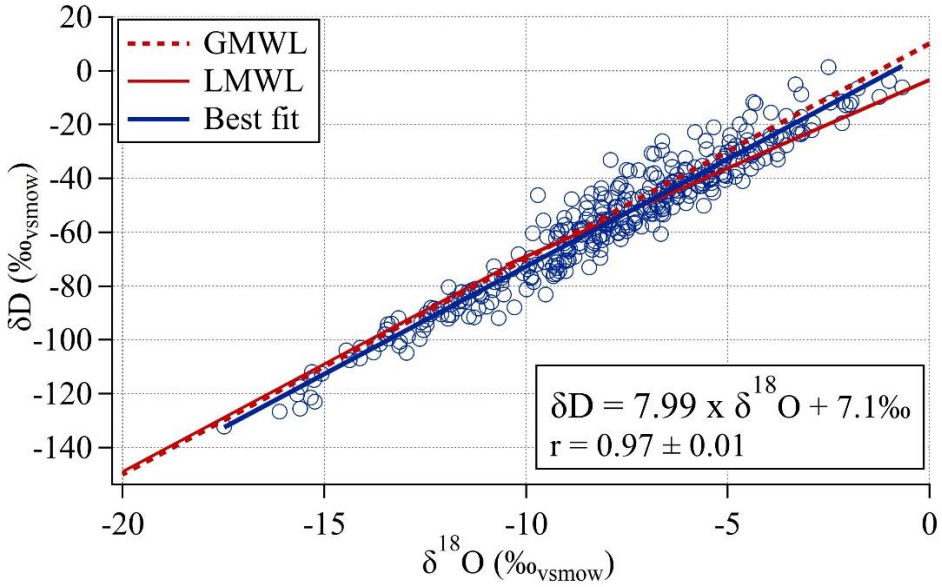

Figure 5.3 The linear relationship (MWL) of $\delta^{18}O$ and δD in the IES isotope data . The blue line is the best fit for the IES isotope dataset, the red dotted line shows the GMWL and the solid red lines show the LMWL for Iceland (Eq. 1.3-1.4).

The best fit for the dataset (δD = 7.99 x $\delta^{18}O$ + 7.1, r = 0.97 ± 0.01) as well as the global and local meteoric water lines for comparison is also shown in the figure. The best fit line has the same slope as the global meteoric water line (GMWL) (Eq. 1.2) but a slightly lower intercept of 7.1 instead of 10 (Figure 5.3). The local meteoric water line (LMWL) for Iceland that expresses the relationship for precipitation with $\delta^{18}O$ values higher or equal to -10.5‰ (Eq. 1.3) has a slope of 6.55 which is a bit lower than the slope of the observed data. The local water line for Iceland expressing values lower or equal to -10.5‰ (Eq. 1.4) has the same slope as the GMWL and the observed data but has higher intercept, 11 instead of 7.1.

5.2 Seasonal variations in the IES isotope data

To investigate further the seasonal effect, the data was split up into 4 different seasons, spring (March, April and May, MAM), summer (June, July and August, JJA), autumn (September, October and November, SON) and winter (December, January and February, DJF). Summary for the isotopic values of $\delta^{18}O$ and *d*-excess, calculated mean values with associated standard deviations (SD), minimum and maximum values, for each season are listed in Table 5.3. The mean isotopic values of $\delta^{18}O$ are most enriched during spring and summer and most depleted during winter while the *d*-excess values are lowest during summer and highest during winter (Table 5.3). The isotopic seasonal mean of $\delta^{18}O$ varies from (-6.82 ± 2.71) ‰ during spring to (-8.94 ± 3.18) ‰ during winter, while the mean for the total dataset is -7.87‰ ± 3.10 (Table 5.3). A much larger variability and higher SD is seen in the mean *d*-excess values, which vary between (2.9 ± 3.4) ‰ in the summer to (10.3 ± 6.3) ‰ during winter where the mean value for the total dataset is (7.2 ± 6.6) ‰ (Table 5.3).

Table 5.3 Mean values and associated standard deviations, minimum and maximum values for the observed IES isotope data , $\delta^{18}O$ and d-excess (‰), by season.

Seasons	**N**	**$\delta^{18}O$ (‰VSMOW)**			**d-excess (‰VSMOW)**		
		Mean ± SD	Min.	Max.	Mean ± SD	Min.	Max.
Spring (MAM)	59	-6.82 ± 2.71	-15.06	-0.67	6.7 ± 6.9	-5.5	23.7
Summer (JJA)	71	-7.22 ± 2.72	-15.60	-2.07	2.9 ± 3.4	-7.2	10.9
Fall (SON)	130	-8.01 ± 3.20	-16.11	-1.78	7.6 ± 6.7	-7.5	26.8
Winter (DJF)	84	-8.94 ± 3.18	-17.48	-1.00	10.3 ± 6.3	0.0	31.4
Total data	344	-7.87 ± 3.10	-17.48	-0.67	7.2 ± 6.6	-7.5	31.4

N: Number of observation days

The distribution of $\delta^{18}O$ and *d*-excess values are displayed in histograms and boxplots (Figure 5.4 - 5.7) showing that the distribution of $\delta^{18}O$ values during spring, summer and fall is approximately Gaussian, while the distribution during the winter months (DJF) is more skewed (Figure 5.4 and 5.5).

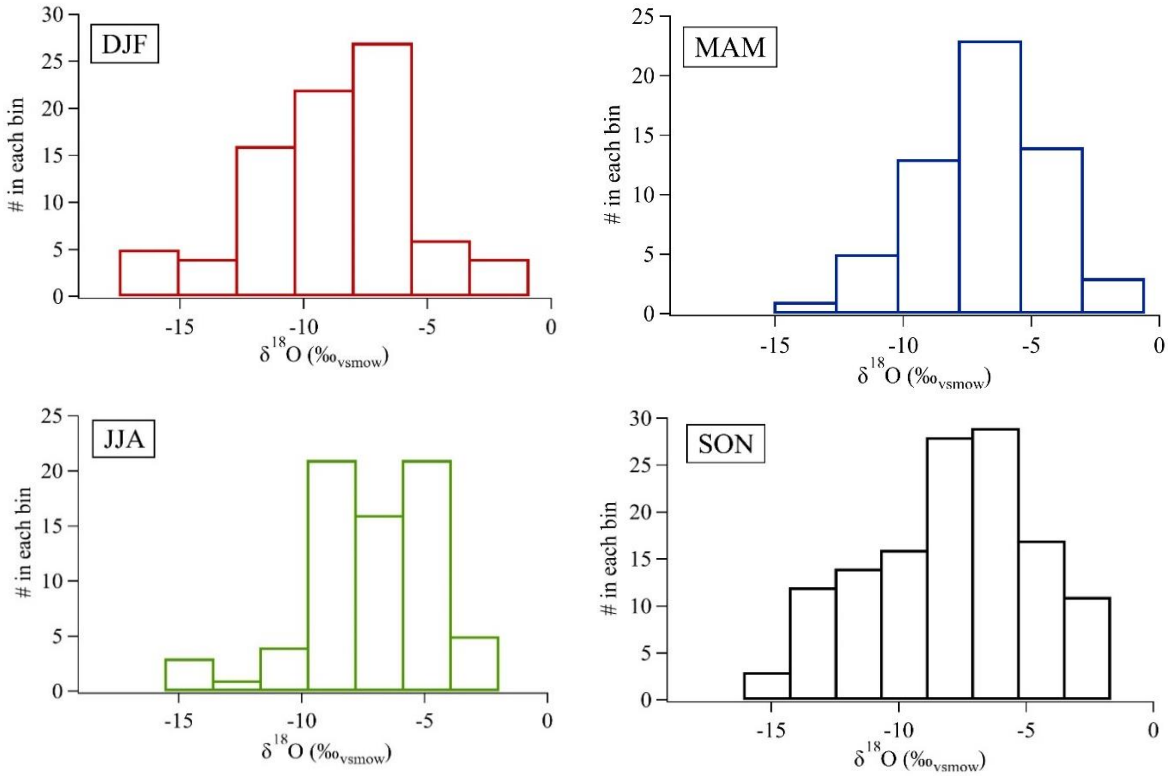

Figure 5.4 Distribution of $\delta^{18}O$ for winter (DJF, red), spring (MAM, blue), summer (JJA, green) and fall (SON, black).

A boxplot gives a good indication of how the values are spread out and shows any outliers in the dataset, represented by dots. The largest range in $\delta^{18}O$ values is observed in the fall, but smaller range is seen during spring and summer (Figure 5.5).

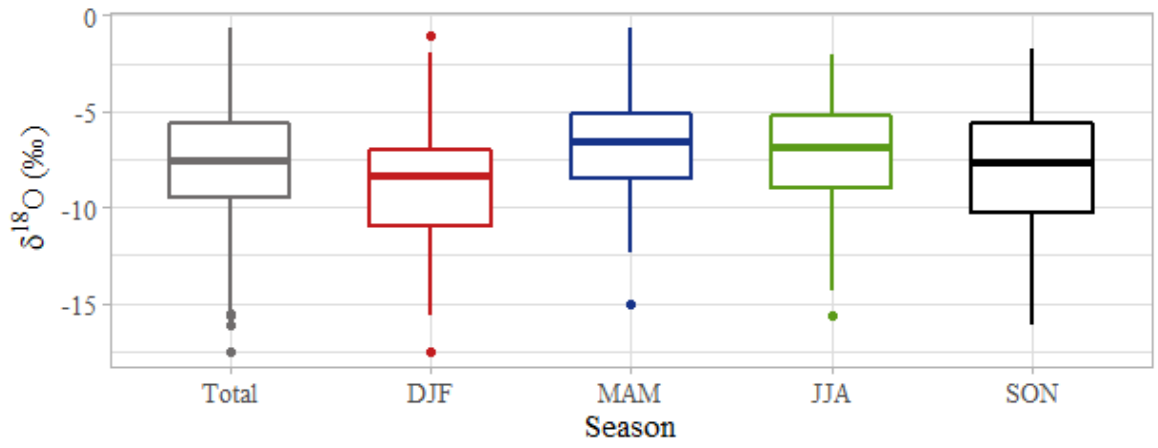

Figure 5.5 Boxplot of $\delta^{18}O$ values, for all seasons.

The distribution of *d*-excess values during winter and fall is approximately Gaussian, while the values in spring and summer show more skewed distribution (Figure 5.6).

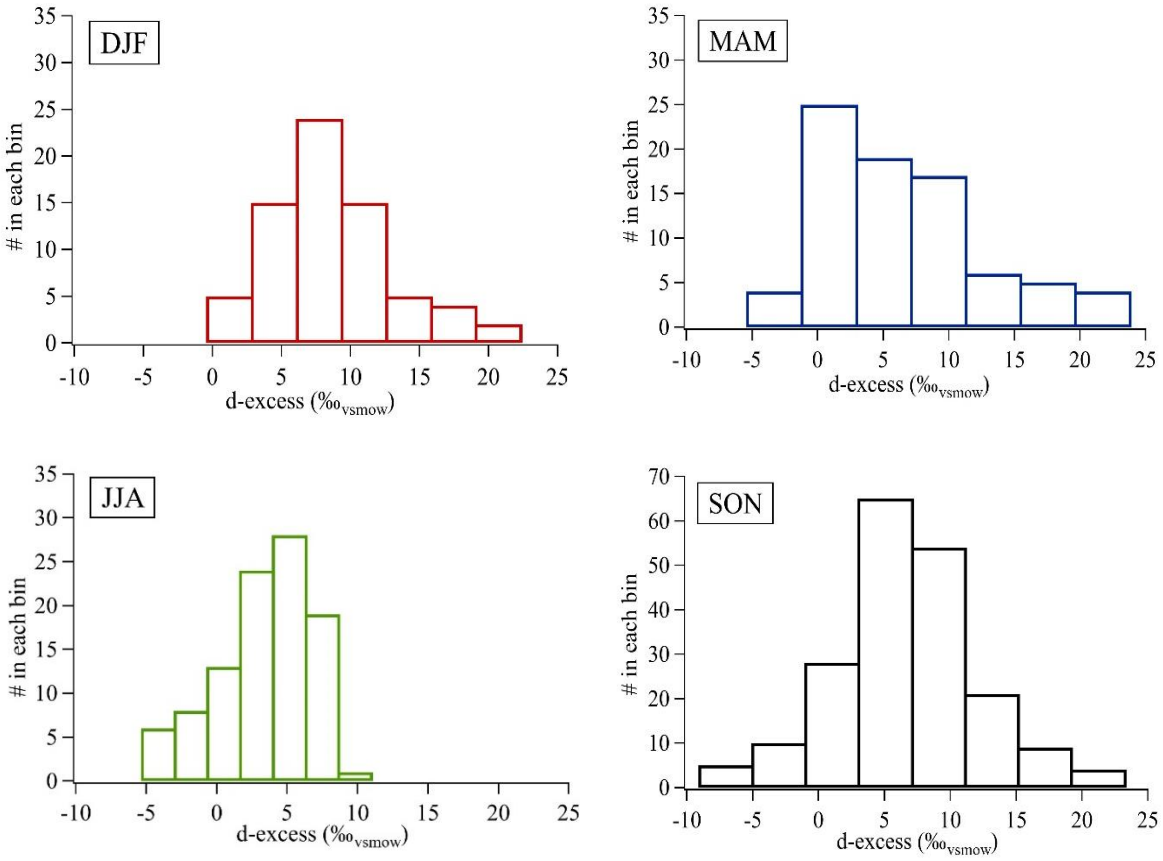

Figure 5.6 Distribution of d-excess for winter (DJF, red), spring (MAM, blue), summer (JJA, green) and fall (SON, black).

As for the $\delta^{18}O$ values, the largest range in *d*-excess values is seen in the fall, but the distribution is also large in the spring. The smallest range on the other hand is seen during

summer (Figure 5.6 - 5.7). The range of *d*-excess values is also small during winter which is different from what is seen for the $\delta^{18}O$ values (Figure 5.5).

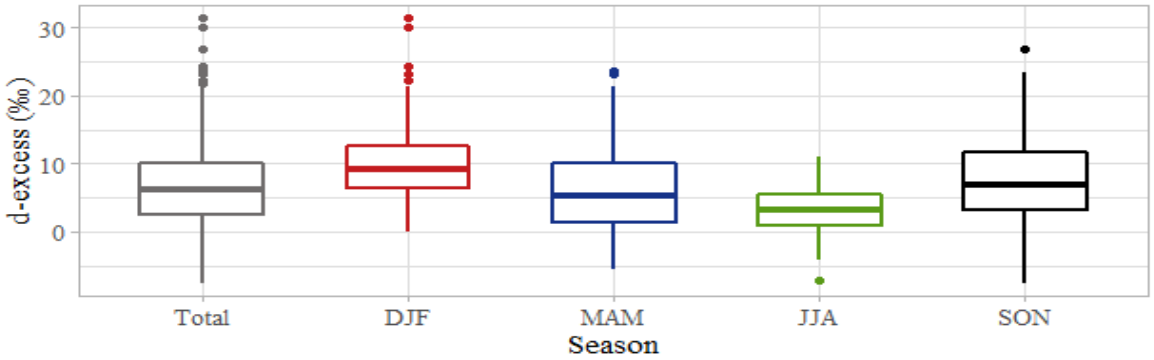

Figure 5.7 Boxplot of d-excess values, for all seasons.

The relationship between $\delta^{18}O$ and δD, is a useful tool to compare seasonal isotopic variations. Local Meteoric Water Lines (LMWL) of isotopic values, were constructed using a linear regression model (Figure 5.8).

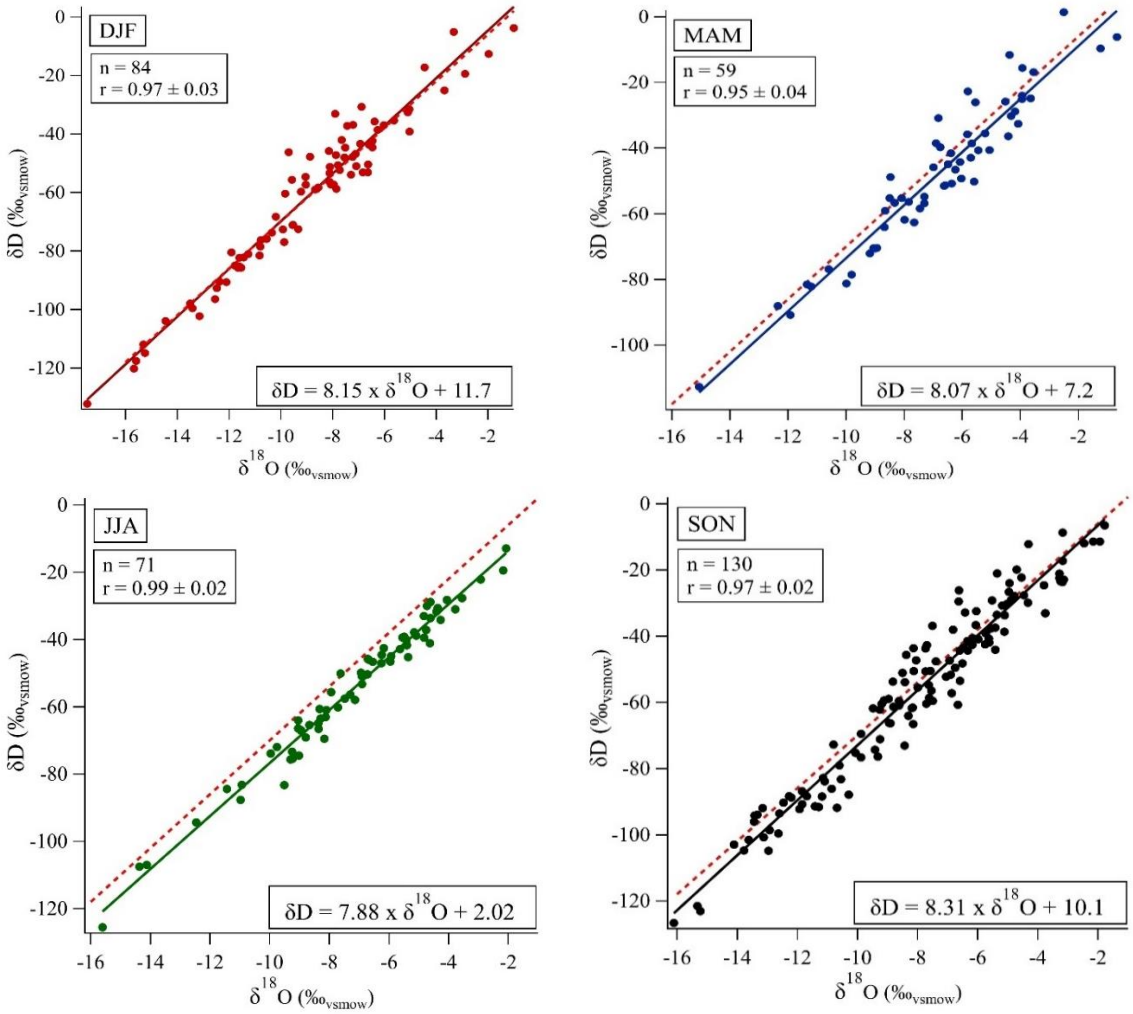

Figure 5.8 Seasonal MWL for IES isotope data. Dashed red line represents the GMWL.

The seasonal water lines were also compared with the Global Meteoric Water Line (GMWL), $\delta D = 8 \times \delta^{18}O + 10$ (Craig, 1961). The MWLs for winter and spring have similar slope as the GLMW, 8.15 and 8.07, respectively (Figure 5.8). A slightly lower slope is seen during summer (7.88) and the highest slope (8.31) is seen in the fall (Figure 5.8). Very strong correlation is observed between $\delta^{18}O$ and δD for all seasons (r from 0.95 to 0.99) (Figure 5.8). Further results for calculated linear regression between isotopic and meteorological data are listed in Table 5.4.

Table 5.4 Linear regression results (slope and correlation coefficients – r and p-values) for observed IES isotope data and IMO meteorological data, by seasons.

Slope IES / IMO data	**DJF**	**MAM**	**JJA**	**SON**
$\delta^{18}O$ vs. temperature	-9.88 ± 0.47 r = 0.31 ± 0.11 p < .005	-8.18 ± 0.74 r = 0.27 ± 0.13 p = .042	-10.09 ± 2.16 r = 0.16 ± 0.12 p = .184	-8.85 ± 0.66 r = 0.12 ± 0.09 p = .165
$\delta^{18}O$ vs. humidity	-11.81 ± 1.50 r = 0.21 ± 0.11 p = .053	-10.11 ± 1.67 r = 0.26 ± 0.13 p = .048	-10.48 ± 2.15 r = 0.18 ± 0.12 p = .129	-9.81 ± 1.25 r = 0.13 ± 0.09 p = .145
$\delta^{18}O$ vs. precipitation	-8.66 ± 0.51 r = -0.09 ± 0.11 p = .442	-6.42 ± 0.46 r = -0.17 ± 0.13 p = .194	-6.43 ± 0.37 r = -0.40 ± 0.11 p < .001	-7.70 ± 0.37 r = -0.11 ± 0.09 p = .193
d-excess vs. temperature	13.2 ± 0.86 r = -0.47 ± 0.10 p < .001	14.49 ± 1.57 r = -0.60 ± 0.11 p < .001	3.73 ± 2.74 r = -0.04 ± 0.12 p = .762	16.08 ± 1.11 r = -0.60 ± 0.07 p < .001
d-excess vs. humidity	27.61 ± 2.35 r = -0.64 ± 0.08 p < .001	24.82 ± 3.65 r = -0.56 ± 0.11 p < .001	0.48 ± 2.72 r = 0.11 ± 0.12 p = .37	21.97 ± 2.3 r = -0.49 ± 0.08 p < .001
d-excess vs. precipitation	11.61 ± 0.99 r = -0.20 ± 0.11 p = .075	6.2 ± 1.19 r = 0.09 ± 0.13 p = .519	2.44 ± 0.50 r = 0.19 ± 0.12 p = .112	7.78 ± 0.78 r = -0.03 ± 0.09 p = .756
Humidity vs. temperature	3.40 ± 0.11 r = 0.66 ± 0.08 p < .001	3.07 ± 0.16 r = 0.81 ± 0.08 p < .001	1.41 ± 0.50 r = 0.78 ± 0.08 p < .001	2.89 ± 0.12 r = 0.87 ± 0.04 p < .001

The uncertainty on the slope represents the standard deviation and the uncertainty on the correlation coefficient represents the standard error.

The strongest correlation for the total IES isotope dataset is seen between *d*-excess values and temperature and specific humidity while $\delta^{18}O$ values show weaker correlation to those meteorological variables (Table 5.2), however, this correlation differs between seasons (Table 5.4). $\delta^{18}O$ values show significant correlation to temperature and specific humidity in winter and spring but not in the summer and fall (Table 5.4). Moderate significant anti-correlation is seen between $\delta^{18}O$ and precipitation amount during summer (r = -0.40 ± 0.11, $p < .001$) but no correlation is observed in other seasons (Table 5.4). The correlation between *d*-excess values and temperature and specific humidity is non-existing during summer (r = -0.04 ± 0.12 and 0.11 ± 0.12, respectively, $p > .05$), but shows strong

significant correlation in all other seasons (Table 5.4). The correlation between the meteorological variables, temperature and specific humidity, also shows variability between seasons, with correlation from $r = 0.66 \pm 0.08$ during winter to $r = 0.87 \pm 0.04$ in the fall (Table 5.4). The mean values and associated standard deviation (SD) for temperature and specific humidity are summarized in Table 5.5.

Table 5.5 Mean values and associated standard deviations, minimum and maximum values for temperature and specific humidity during observation days (data from IMO), by seasons.

Seasons	**N**	**Temperature (°C)**			**Specific humidity (g/kg)**		
		Mean ± SD	Min.	Max.	Mean ± SD	Min.	Max.
Spring (MAM)	59	5.9 ± 3.1	-0.7	10.7	4.5 ± 1.0	2.1	6.3
Summer (JJA)	71	11.0 ± 1.7	7.7	16.1	6.5 ± 1.0	4.5	8.9
Fall (SON)	130	6.7 ± 3.2	-1.4	12.8	5.0 ± 1.2	2.4	7.9
Winter (DJF)	84	2.8 ± 2.9	-6.0	8.4	4.0 ± 1.0	1.5	6.3
IMO total	344	6.5 ± 3.9	-6.0	16.1	5.0 ± 1.4	1.5	8.9

N: Number of observation days

The distribution for temperature and specific humidity are further shown in boxplots (Figure 5.9).

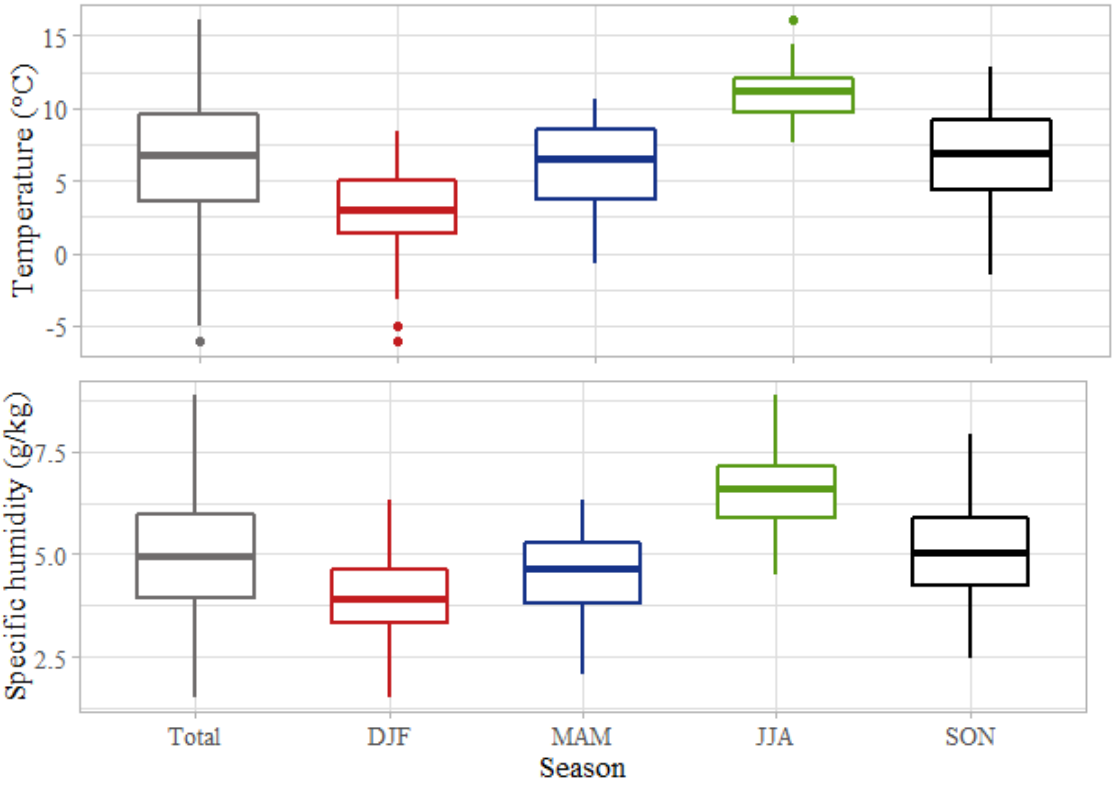

Figure 5.9 Boxplots for temperature and specific humidity (data from IMO), for all seasons.

The results are similar for specific humidity and temperature for all seasons except summer, where the range for specific humidity is larger (Figure 5.9).

5.3 Precipitation event on 18 September 2019

Sampling from one low pressure event on 18 September 2019 was done every 30 minutes from 9:00 in the morning until 14:30 in the afternoon, when the rain event had passed Reykjavík, resulting in 12 samples (Appendix B). The isotopic values from the collected samples plotted on a timeline together with meteorological data from the IMO (Figure 5.10) show that the isotopic values for $\delta^{18}O$ and δD become more enriched during the warm front passage and the temperature and humidity values show the same increase. At the same time *d*-excess values are decreasing (Figure 5.10). The precipitation amount varies during the front passage but a drop in precipitation is observed at 09:30, 12:00 and 13:30, which is also observed in the *d*-excess values, most distinctively at 12:00 when the precipitation amount dropped significantly (Figure 5.10). At the same time, there is a slight increase in the $\delta^{18}O$ values suggesting some relationship between $\delta^{18}O$ values and the precipitation amount, but the calculated correlation shows no relationship between the $\delta^{18}O$ values and precipitation ($r = 0.05 \pm 0.32$, $p = .88$) (Table 5.7)

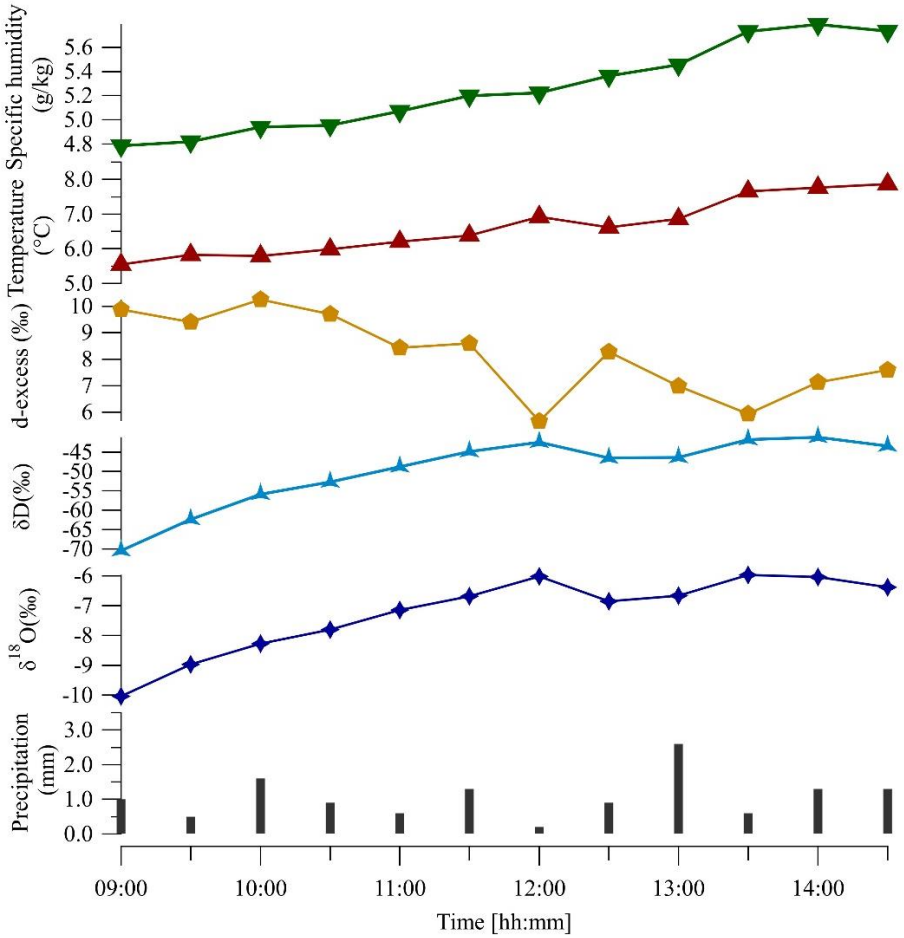

Figure 5.10 Results for $\delta^{18}O$, δD and d-excess plotted on a timeline together with meteorological data from IMO for one precipitation event on 18 September 2019.

The mean values with associated standard deviations, minimum and maximum for samples and meteorological data from IMO are listed in Table 5.6.

Table 5.6 Mean values and associated standard deviations, minimum and maximum values of the observed data from one precipitation event ($\delta^{18}O$, δD and d-excess), temperature, specific and relative humidity and precipitation amount (data from IMO).

18 September 2019	**IES / IMO data**	**Min.**	**Max.**
$\delta^{18}O$ (‰)	-7.24 ± 9.09	-10.04	-5.97
δD (‰)	-49.8 ± 9.1	-70.5	-41.2
d-excess (‰)	8.2 ± 1.5	5.7	10.3
Temperature (°C)	6.6 ± 0.8	5.6	7.9
Specific humidity (g/kg)	5.3 ± 0.4	4.8	5.8
Precipitation (mm)	1.1 ± 0.8	0.2	2.6

The temperature increased from 5.6 °C to 7.9 °C during the sampling time and the specific humidity increased from 4.8 to 5.8 g/kg during same time (Figures 5.10 and 5.11, Table 5.6). The precipitation also varied during the sampling period (Figure 5.10), with minimum of 0.2 mm in 30 minutes up to 2.6 mm in 30 minutes (Table 5.6).

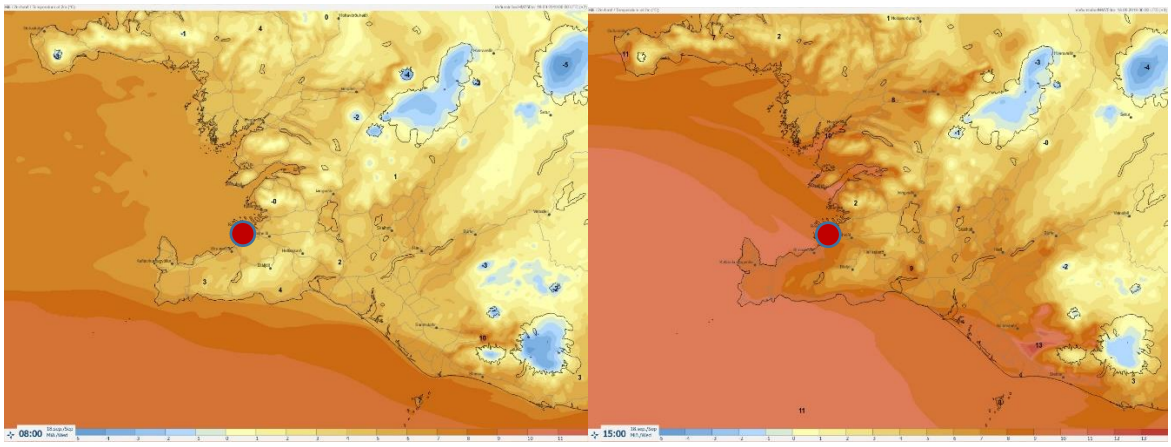

Figure 5.11 Temperature at the sampling site at 8:00 (left) and at 15:00 (right) on September 18th 2019 (Veðurstofa Íslands, 2019b).

Although the sampling only took place over 5 and a half hour's period, a considerable variability is seen in the isotopic values (Figure 5.10, Table 5.6). The correlation between $\delta^{18}O$ and both temperature and specific humidity is strong with (r = 0.84 ± 0.17, p < .001) (Table 5.7). Same strong correlation is also seen between δD values and temperature (r = 0.82 ± 0.18) and specific humidity (r = 0.83 ± 0.18), while a significant strong anti-correlation is seen *b*etween d-excess values and temperature (r = -0.81 ± 0.19, p = .001) and specific humidity (r = -0.76 ± 0.21, p = .004) (Table 5.7). The precipitation amount does not seem to have any correlation to the $\delta^{18}O$ values (r = 0.05 ± 0.32) nor the *d*-excess values (r = 0.10 ± 0.31), however the *d*-excess value dropped by about 3‰ around noon, when the precipitation amount dropped significantly. The $\delta^{18}O$ and δD values level off at the same time (Figure 5.10).

Table 5.7 Linear regression results (correlation coefficients – r and p-values) for observed IES istotope data and IMO meteorological data, One event, 18 September 2019.

	Temperature (°C)	**Specific humidity (g/kg)**	**Precipitation (mm)**
d-excess (‰)	r = -0.81 ± 0.19	r = -0.76 ± 0.21	r = 0.10 ± 0.31
	p = .001	p = .004	p = .765
δD (‰)	r = 0.82 ± 0.18	r = 0.83 ± 0.18	r = 0.07 ± 0.32
	p = .001	p = .001	p = .825
$\delta^{18}O$ (‰)	r = 0.84 ± 0.17	r = 0.84 ± 0.17	r = 0.05 ± 0.32
	p < .001	p < .001	p = .88

The uncertainty on the correlation coefficient represents the standard error.

6 Discussion

6.1 IES isotope data

This is the first study in Iceland where daily precipitation has been collected over a longer period and isotopic values measured. Few studies of variations in daily precipitation isotope content are available (Bedaso & Wu, 2020; Fujita & Abe, 2006) while many studies are based on monthly isotopic data from the GNIP database (Ichiyanagi, 2007). Precipitation results from Iceland show that there is strong seasonality in the isotopic data and the relationships between isotopic values and meteorological data vary between seasons.

Few studies have specifically investigated the characteristic isotope signature of frontal passages, which are typically associated with intense precipitation (Aemisegger et al., 2015; Dansgaard, 1953; S Pfahl, Wernli, & Yoshimura, 2012). In accordance with Celle-Jeanton, Gonfiantini, Travi, and Sol (2004) and Muller, Baker, Fairchild, Kidd, and Boomer (2015), the passage of warm front over Reykjavík on September 18th2019 shows strong intra-event variability in isotopic values over a short period of time and a clear relationship of the isotopic values to temperature and specific humidity. A warm front is defined as the transition zone where warmer air mass is replacing colder air mass, resulting in warmer and more humid conditions (Sodemann, 2006). Earlier studies show that warm fronts are associated with transport of warm and moist air above a relatively cold air mass resulting in some of its vapor condensing. As the front passes, an increase can be observed in the precipitation δ-values over time at a specific place (Dansgaard, 1953; S Pfahl et al., 2012; Sodemann, 2006). This is in accordance with the observed isotopic composition of the precipitation samples collected from the low-pressure front passing Reykjavík on September 18th2019 and what is interesting here is how much the isotopic values of $\delta^{18}O$ and δD change (from -10.04‰ to -5.97‰ and from -70.5‰ to -41‰, respectively) in relatively short period of time (5 hours). The visible decrease in the *d*-excess values around noon and around 13:30, when precipitation drops significantly suggests a correlation between the *d*-excess values and precipitation amount, but when the whole dataset is taken into consideration statistical calculation show no correlation between those variables. It is essential to sample from more frontal passages, both warm and cold, to better understand the parameters that control events at this scale.

6.2 Monthly cumulative sampling versus daily sampling of precipitation

Isotopic values for cumulative monthly samples of precipitation in Reykjavík, sampled by the Icelandic Meteorological Office (IMO) and measured at the Institute of Earth Sciences (IES) are available for the whole sampling period. The isotopic results of those monthly samples are presented on a timeline in comparison with the daily IES precipitation samples as well as their weighted monthly mean, over the period from July 2016 to February 2020 (Figure 6.1). Linear regression results between the calculated monthly averages of the daily precipitation samples and IMO monthly samples, excluding May 2018 and February 2019 (due to lack of IES isotope data), are presented in Table 6.5.

Table 6.1 Linear regression (correlation coefficient – r and p-values) for monthly average of IES isotopic data and monthly cumulative samples from IMO.

IES / IMO monthly	**Correlation coefficient - *r***	***P* - value**
d-excess (‰)	$r = 0.53 \pm 0.13$	$p < .001$
δD (‰)	$r = 0.78 \pm 0.1$	$p < .001$
$\delta^{18}O$ (‰)	$r = 0.78 \pm 0.1$	$p < .001$

The uncertainty on the correlation coefficient represents the standard error.

A significant strong correlation is seen between the calculated monthly averages of daily sampling and the monthly samples from IMO for $\delta^{18}O$ and δD ($r = 0.78 \pm 0.1$, $p < .001$) and moderate correlation is seen in *d*-excess values ($r = 0.53 \pm 0.13$, $p < .001$) (Table 6.1). The daily sampling shows a large variability that is smoothed out in the monthly IES isotopic averages or the IMO monthly samples (Figure 6.1). The most distinctive difference between the monthly isotopic datasets, especially in *d*-excess values, is during summer of 2017, reported to be unusually dry in Reykjavík (Veðurstofa Íslands, 2018) and in March-April 2018, also reported to have precipitation below average (Veðurstofa Íslands, 2019d) (Figure 6.1)

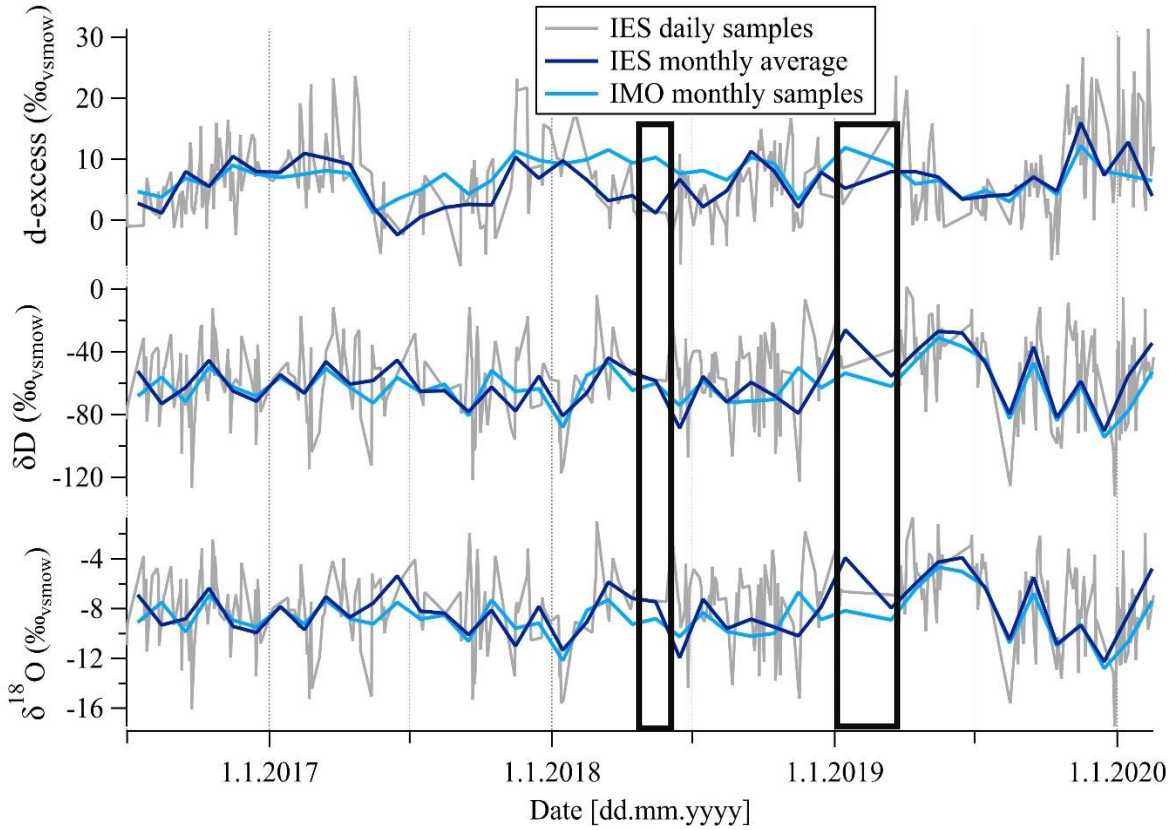

Figure 6.1 Comparison of isotopic values between daily and monthly averages of IES isotope data and monthly samples from IMO ($\delta^{18}O$, δD and d-excess). The boxes outline gaps in the IES isotope data.

As to be expected, there is a large difference between the datasets where there are gaps in the IES dataset (May 2018 and February 2019) (Figure 6.1). This is a bias that needs to be considered when interpreting the data and those months are not included in the linear regression calculation. May 2018 is for instance reported to have had precipitation way above average with the most precipitation amount since the beginning of measurements in Reykjavík (Veðurstofa Íslands, 2019d).

6.3 Comparison to ECHAM5-wiso GCM

Parameterization of water isotopes in the hydrological cycle is implemented in isotope-enabled climate models such as the ECHAM5-wiso general circulation model. To investigate how well the model captures observed isotopic variations the isotopic values, $\delta^{18}O$ (‰), δD (‰) and *d*-excess (‰), precipitation amount (mm), temperature (°C) and specific humidity (g/kg) from the model was used to compare to the Reykjavík observations. The ECHAM5-wiso data has 6-hour interval, covering the period from 1 January 2010 until 31 December 2018. However, the IES precipitation sampling started on June 30th2016 and thus only the overlapping period between the observation and the model data (30 June 2016 to 31 December 2018) was extracted and used for the comparison, a total of 222 observation days (Appendix C). The data was extracted from netCDF files using R language (Team, 2013) from a grid point with latitude 64.1°N and longitude 338.1°E, the approximate coordinates for Reykjavík, Iceland. ECHAM5 has horizontal resolution that corresponds to ~3.75°x 3.75° (Roeckner et al., 2003). A bilinear option was used to interpolate values from the four nearest cells. A weighted mean for every 24 hours was calculated from the 6-hour isotopic values extracted from the ECHAM5-wiso model, using the precipitation amount. 24-hour average was calculated for temperature and specific humidity, and the sum of 24-hour for precipitation amount. Summary for the extracted ECHAM5-wiso data is listed in Table 6.2.

Table 6.2 Daily mean values and associated standard deviations, minimum and maximum values of the ECHAM5-wiso simulation data, $\delta^{18}O$, δD, d-excess, temperature, specific humidity and precipitation.

	ECHAM5-wiso	**Min.**	**Max.**
$\delta^{18}O$ (‰)	-8.08 ± 3.50	-18.32	-1.10
δD (‰)	-57.3 ± 28.4	-138.9	0.1
d-excess (‰)	7.3 ± 3.4	-1.4	17.7
Temperature (°C)	6.2 ± 3.3	-3.4	12.8
Specific humidity (g/kg)	5.3 ± 1.3	2.3	9.1
Precipitation (mm)	7.3 ± 6.8	0.1	38.0

The distribution of isotopic values ($\delta^{18}O$, δD and *d*-excess) and meteorological data (temperature, specific humidity and precipitation amount) from the ECHAM5-wiso model is displayed in histograms in Figure 6.2.

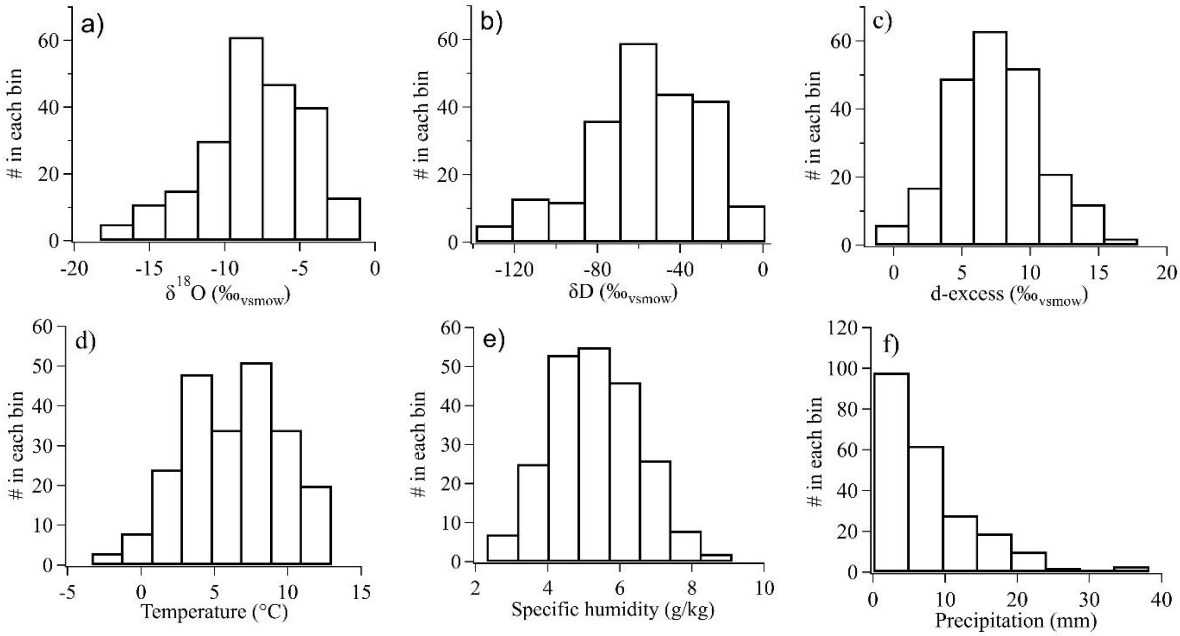

Figure 6.2 Distributions of $\delta^{18}O$ (a), δD (b), d-excess (c), temperature (d), specific humidity (e) and precipitation (f) values from the ECHAM5-wiso simulation.

Comparison between the mean values and associated standard deviation for ECHAM5-wiso data and observed IES isotope data is displayed in Table 6.3. The $\delta^{18}O$ has the same mean value (-8.08‰) for both datasets and difference of 1‰ between mean δD values and difference of 0.9‰ between mean *d*-excess values (Table 6.3). The mean temperature from ECHAM5-wiso is 0.8 °C below the observed data but the specific humidity has similar values for both datasets, only 0.2 g/kg difference in the mean values. The largest difference between the average mean of ECHAM5-wiso and observed values is in the precipitation amount (2.5 mm or 34%) (Table 6.3).

Table 6.3 Comparison of daily mean values and associated standard deviations, ECHAM5–wiso and observed IES isotope data, daily mean $\delta^{18}O$, δD, d-excess, temperature, specific humidity and precipitation.

	ECHAM5-wiso	**IES / IMO data**
$\delta^{18}O$ (‰)	-8.08 ± 3.50	-8.08 ± 2.99
δD (‰)	-57.3 ± 28.4	-58.3 ± 24.4
d-excess (‰)	7.3 ± 3.4	6.4 ± 5.9
Temperature (°C)	6.2 ± 3.3	7.0 ± 3.6
Specific humidity (g/kg)	5.3 ± 1.3	5.1 ± 1.2
Precipitation (mm)	7.3 ± 6.8	4.8 ± 6.5

The classical Taylor diagrams (Taylor, 2001), developed for model evaluation and model-inter comparison, were used to provide quantitative information on how good the ECHAM5-wiso model is in simulating the day-to-day isotopic variability (Figure 6.3, left panel). The Taylor diagrams show the correspondence between the modelled and observed data in three terms of statistics: the Pearson correlation coefficient, the root-mean-square

error (RMSE) and the standard deviation (SD). The direct linear relationship between the model outputs and observations were plotted as well (Figure 6.3, right panel). Both $\delta^{18}O$ and *d*-excess values show significant ($p < .001$) correlation with $r = 0.63 \pm 0.05$ and $r = 0.48 \pm 0.06$, respectively (Figure 6.4).

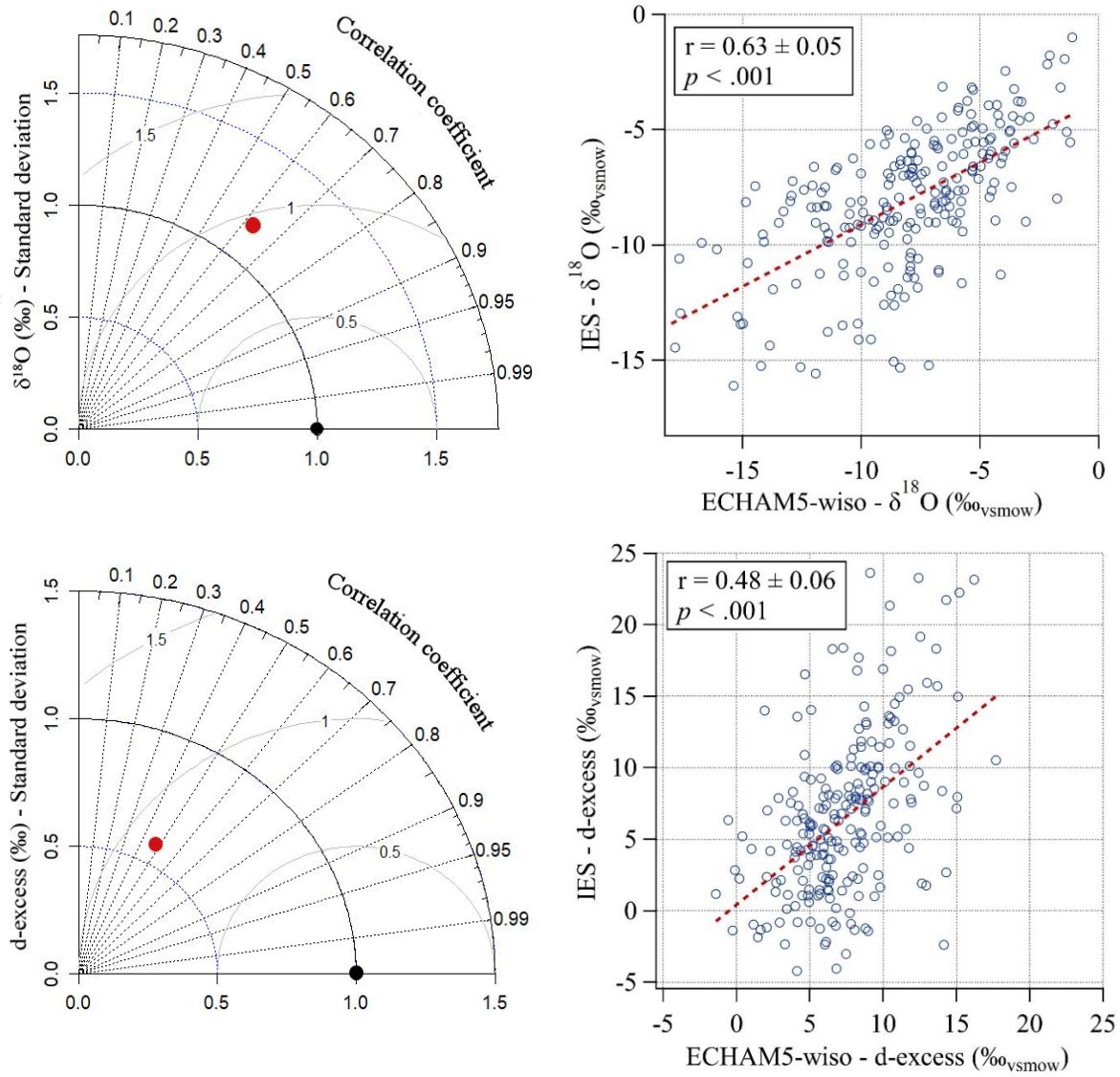

Figure 6.3 Taylor diagrams showing the normalized standard deviation and the correlation coefficient for ECHAM5-wiso(red dot) with the observed IES isotope data (black dot) (from top to bottom: $\delta^{18}O$ and d-excess (‰). The direct comparison of ECHAM5-wiso (x-axis) and IES isotope data (y-axis)(dashed red line) on right panel.

The ECHAM5-wiso model is simulating both temperature and specific humidity very well with very strong significant correlation ($r = 0.91 \pm 0.03$ and $r = 0.93 \pm 0.02$, $p < .001$, respectively) (Figure 6.4). There is also strong significant correlation in precipitation amount between the observed and modelled data ($r = 0.67 \pm 0.05$, $p < .001$) (Figure 6.4) which shows that ECHAM5-wiso is doing a good job simulating the meteorological variables.

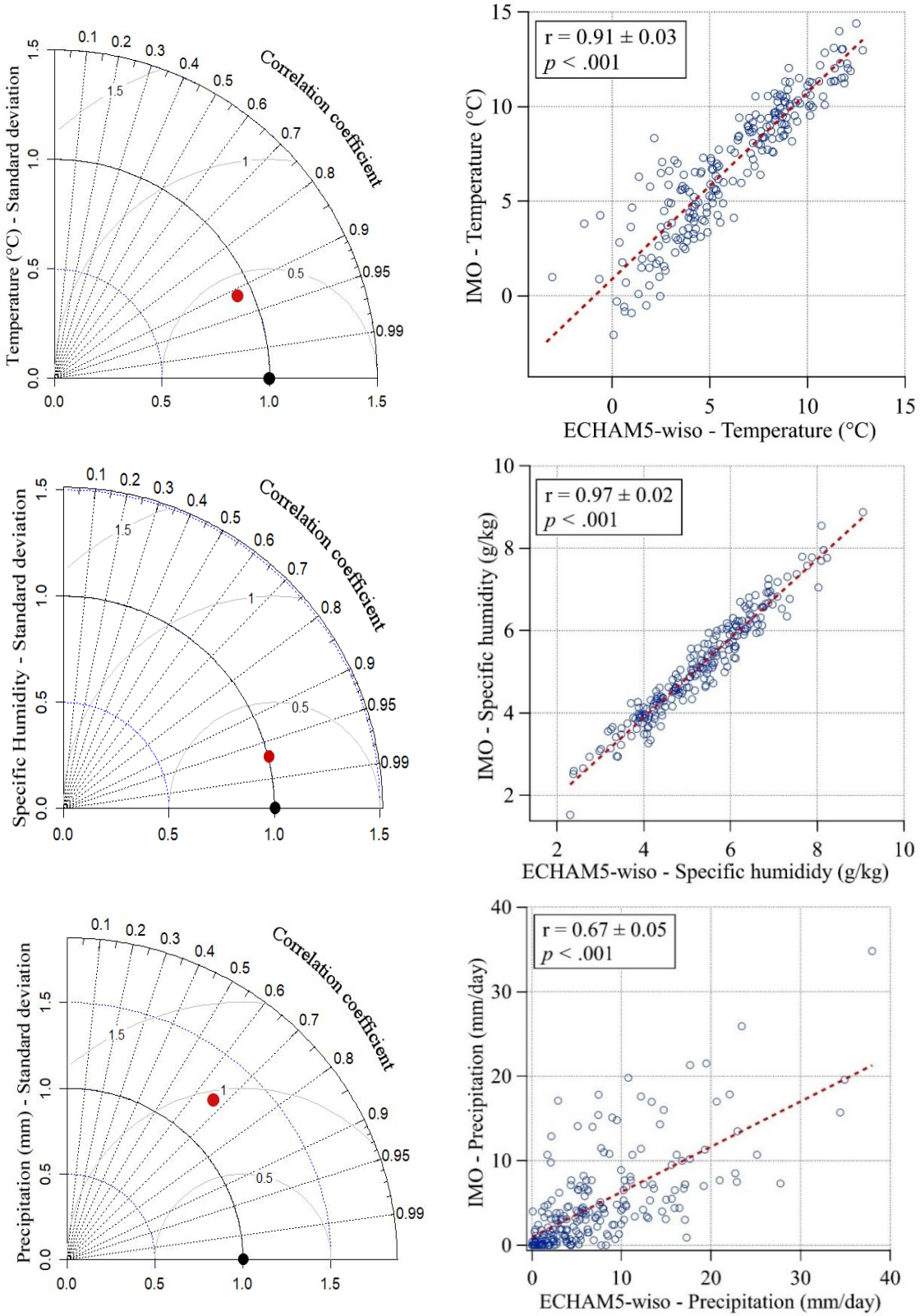

Figure 6.4 Taylor diagrams showing the normalized standard deviation and the correlation coefficient for ECHAM5-wiso (red dot) with meteorological data from IMO (black dot). Direct comparison of ECHAM5-wiso (x-axis) against IMO meteorological data (y-axis) on right panel.

To investigate further possible seasonal differences between the ECHAM5-wiso modelled data and the observed IES isotope data and the IMO meteorological data, the ECHAM5-wiso data was split up into 4 seasons, spring (MAM), summer (JJA), fall (SON) and winter (DJF). The summary for mean values and associated standard deviation for both ECHAM5-wiso and observed data is listed in Table 6.4 and the linear regression results (slope and correlation coefficients, *r* with *p*-values) between datasets are listed in Table 6.5.

Table 6.4 Daily mean values and associated standard deviations for ECHAM5-wiso and IES istotope / IMO meteorological data ($\delta^{18}O$, d-excess, temperature and specific humidity), by season.

Seasons	**N**	**$\delta^{18}O$ (‰) - Mean ± SD**		***d*-excess (‰) - Mean ± SD**	
		ECHAM5-wiso	IES	ECHAM5-wiso	IES
Spring (MAM)	35	-7.49 ± 3.26	-7.52 ± 2.47	6.4 ± 3.6	6.2 ± 6.5
Summer (JJA)	52	-7.07 ± 2.72	-7.45 ± 2.44	5.6 ± 2.0	2.9 ± 3.7
Fall (SON)	92	-8.06 ± 3.40	-8.18 ± 3.28	7.6 ± 3.3	6.9 ± 6.1
Winter (DJF)	43	-9.83 ± 4.15	-9.10 ± 3.10	9.5 ± 3.6	9.8 ± 4.7
Total	222	-8.08 ± 3.50	-8.08 ± 2.99	7.3 ± 3.4	6.4 ± 5.9
		Temperature (°C) - Mean ± SD		**Specific humidity (g/kg) - Mean ± SD**	
		ECHAM5-wiso	IMO	ECHAM5-wiso	IMO
Spring (MAM)	35	4.6 ± 2.7	5.8 ± 2.7	4.7 ± 0.9	4.5 ± 0.8
Summer (JJA)	52	9.7 ± 1.7	10.8 ± 1.7	6.6 ± 0.9	6.5 ± 0.9
Fall (SON)	92	6.2 ± 2.8	6.9 ± 3.0	5.3 ± 1.1	5.1 ± 1.1
Winter (DJF)	43	2.9 ± 1.8	3.4 ± 2.7	4.3 ± 0.8	4.1 ± 0.8
Total	222	6.2 ± 3.3	7.0 ± 3.6	5.3 ± 1.3	5.1 ± 1.2

N: Number of observation days

Some differences can be seen between mean values of the datasets for different seasons. The largest difference in $\delta^{18}O$ is seen during winter (0.73‰) (Table 6.4) The largest difference in *d*-excess values is seen in summer (2.7‰) (Table 6.4). Specific humidity is similar in all seasons for both datasets with mean values of 0.1 - 0.2 g/kg higher than the observed data. There is more difference in the temperature values, where ECHAM5-wiso values are lower in all season, from 0.7°C in the fall up to 1.9 °C during winter (Table 6.4).

Table 6.5 Linear regression results (slope and correlation coefficients - r and p-values) between ECHAM5-wiso simulation and IES isotope data / IMO meteorological data, for $\delta^{18}O$, d-excess, temperature, specific humidity and precipitation, by season.

ECHAM5-wiso vs. IES/IMO	**Spring (MAM)**	**Summer (JJA)**	**Fall (SON)**	**Winter (DJF)**	**Total**
$\delta^{18}O$	-5.17 ± 0.98	3.39 ± 0.74	-3.11 ± 0.68	-4.42 ± 0.96	-3.74 ± 0.39
	r = 0.42 ± 0.16	r = 0.64 ± 0.11	r = 0.65 ± 0.08	r = 0.64 ± 0.12	r = 0.63 ± 0.05
	p = .013	p < .001	p < .001	p < .001	p < .001
d-excess	2.04 ± 2.14	3.6 ± 1.54	0.08 ± 1.41	4.07 ± 1.79	0.39 ± 0.82
	r = 0.36 ± 0.16	r = -0.07 ± 0.14	r = 0.49 ± 0.09	r = 0.47 ± 0.14	r = 0.48 ± 0.06
	p = .033	p = 0.612	p < .001	p = .0015	p < .001
Temperature	1.76 ± 0.49	2.7 ± 0.79	1.17 ± 0.37	0.25 ± 0.56	0.88 ± 0.21
	r = 0.85 ± 0.09	r = 0.83 ± 0.08	r = 0.87 ± 0.05	r = 0.72 ± 0.11	r = 0.91 ± 0.03
	p < .001	p < .001	p < .001	p < .001	p < .001
Specific humidity	0.49 ± 0.30	0.33 ± 0.33	0.21 ± 0.16	0.31 ± 0.21	0.05 ± .09
	r = 0.92 ± 0.07	r = 0.94 ± 0.05	r = 0.96 ± 0.03	r = 0.95 ± 0.05	r = 0.97 ± 0.02
	p < .001	p < .001	p < .001	p < .001	p < .001
Precipitation	0.64 ± 0.71	0.18 ± 0.7	1.12 ± 0.64	2.03 ± 1.29	0.93 ± 0.4
	r = 0.78 ± 0.11	r = 0.56 ± 0.13	r = 0.67 ± 0.08	r = 0.56 ± 0.13	r = 0.67 ± 0.05
	p < .001	p < .001	p < .001	p < .001	p < .001

The uncertainty on the slope represents the standard deviation and the uncertainty on the correlation coefficient represents the standard error.

The calculated correlation between the datasets are shown in Table 6.5. The largest discrepancy is seen in *d*-excess values during summer, where there is no correlation (r = -0.07 ± 0.14, p = .612). The correlation is moderate during other seasons with r = 0.36 ± 0.16 to 0.49 ± 0.09 (Table 6.5). Difference in correlation between seasons is not as clear in the $\delta^{18}O$ values, where a significant strong correlation is seen between the datasets for all seasons (r ~ 0.64, p < .001) except for spring (r = 0.42 ± 0.16, p = .013) (Table 6.5).

Comparison between seasons for the two datasets is further presented in boxplots to demonstrate the spread in values (Figure 6.5). The ECHAM5-wiso simulates the $\delta^{18}O$ values quite well throughout all seasons, except for winter where the simulated data is more spread, and the median is lower than for the observed values. The boxplot for the δD values shows similar results with the largest difference during winter where the model values are lower and more spread than the observed data. The modelled *d*-excess values have less spread and higher median than the observed data in all seasons except winter (Figure 6.5).

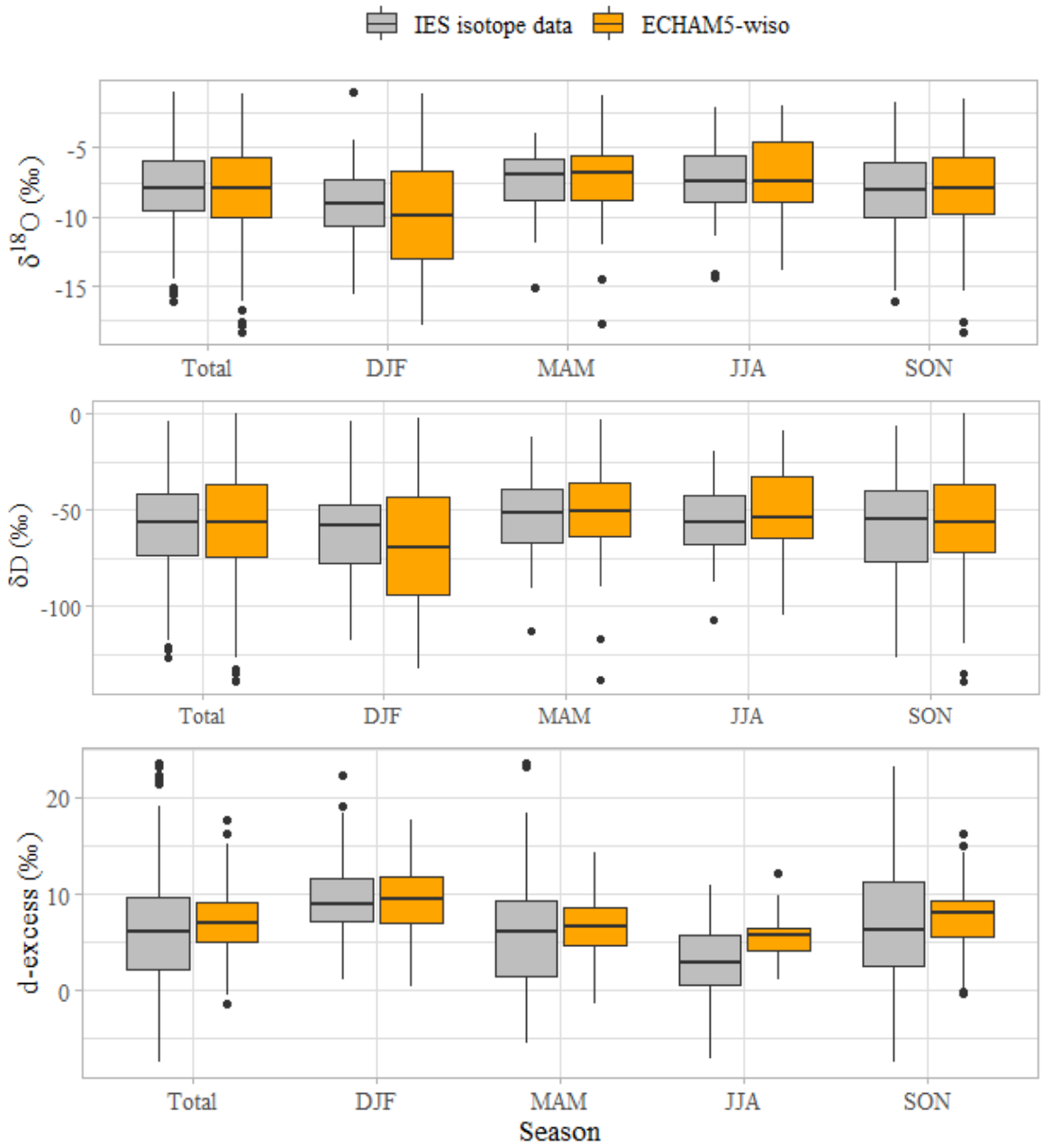

Figure 6.5 Boxplots for comparison of ECHAM5-wiso simulations and observed isotope data IES isotope data, by seasons.

The boxplots in Figure 6.6 demonstrate that the ECHAM5-wiso is simulating specific humidity well in all seasons, with a slightly higher median during spring and fall. The mean temperature is slightly underestimated in the ECHAM5-wiso model in all seasons, with the largest difference in spring and summer, while the precipitation amount is overestimated in the model compared to the observed data in all seasons (Figure 6.6).

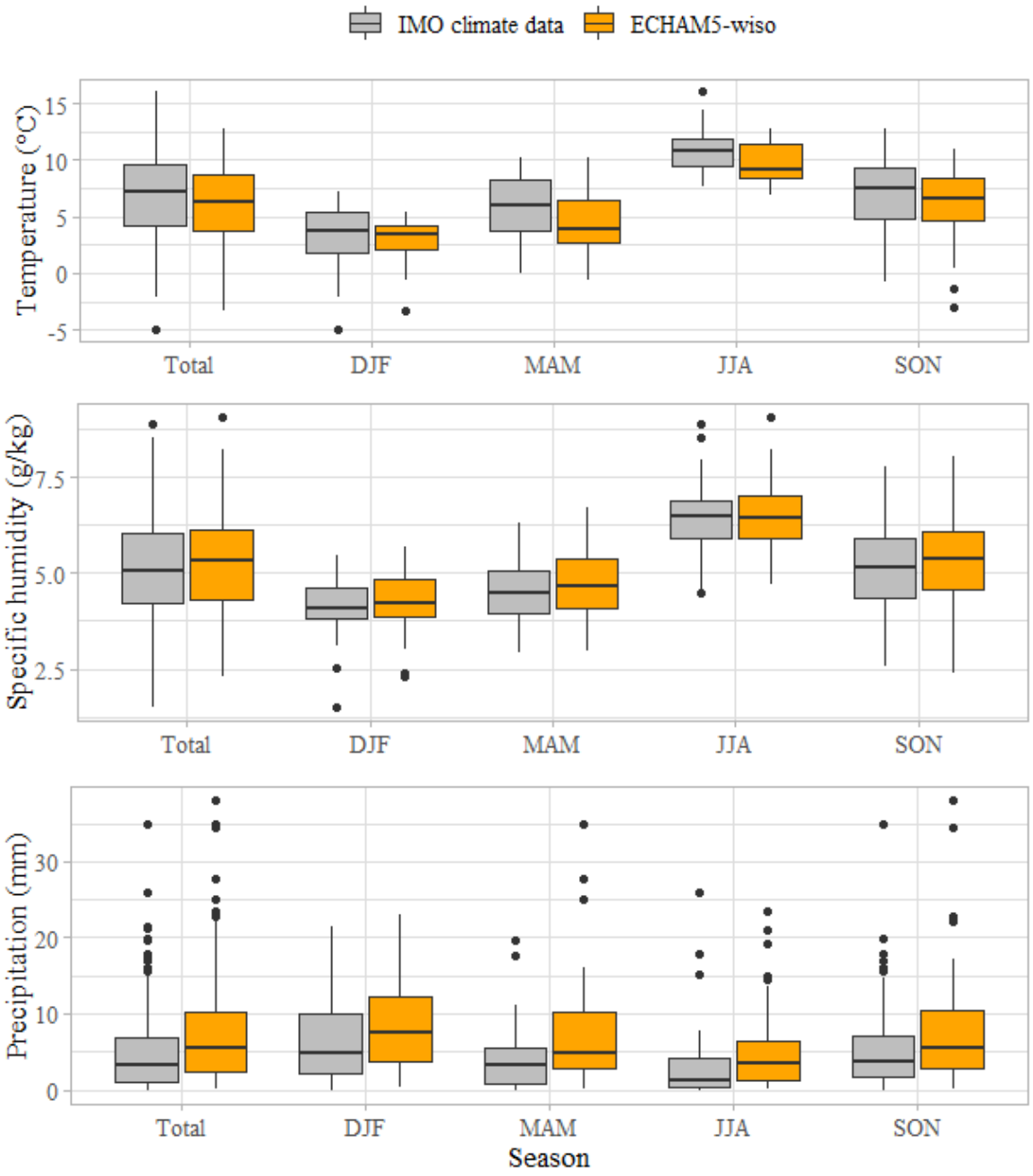

Figure 6.6 Boxplots for comparison of ECHAM5-wiso simulations and observed meteorological data (from IMO), by seasons.

Steen-Larsen, Risi, Werner, Yoshimura, and Masson-Delmotte (2017), evaluated how well different isotope-enabled general circulation models, concluding that the ECHAM5-wiso model, were performing and their conclusion was that the ECHAM5-wiso was doing poorly for *d*-excess values, better for $\delta^{18}O$ values and very good for temperature and humidity, which is in agreement with the results from this study.

6.4 NAO index comparison

In this section the possible relationship between the NAO index and measured isotopic values is investigated. The plotted NAO index from July 2016 to February 2020 shows that the index is more positive than negative during this period, with a negative phase from May to October 2019 (Figure 6.7).

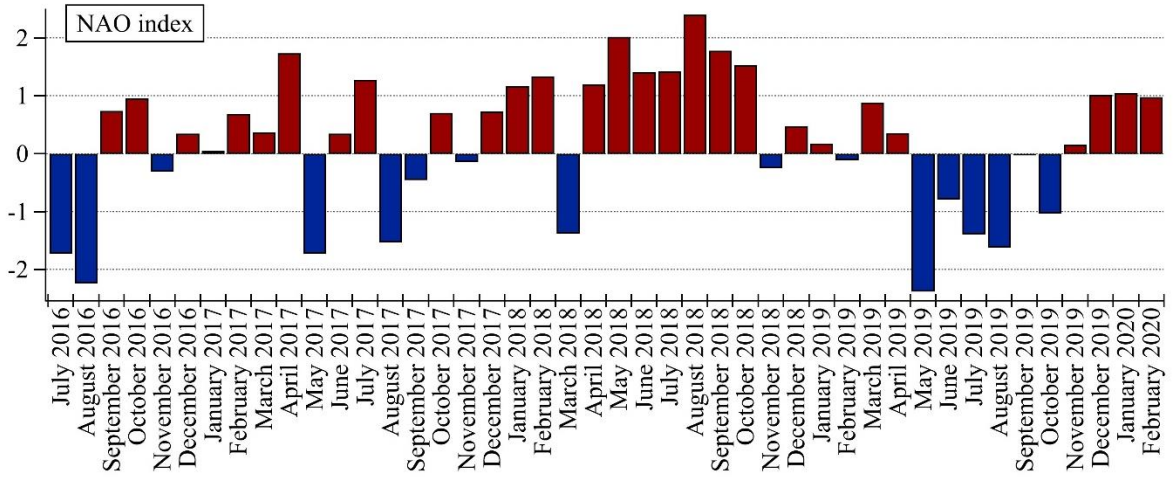

Figure 6.7 The NAO index from July 2016 to February 2020 (NOAA, 2020)

Linear regression was used to calculate the slope and correlation between the NAO index and the calculated monthly averages for the IES as well as the monthly samples from IMO, both for the total datasets, and also for only the winter months (DJF) since the NAO is most prominent during those months. The results are summarized in Table 6.6. Weak anti-correlation is found between the NAO index and the $\delta^{18}O$ values when the whole datasets (42 months) are considered (r = -0.21 ± 0.15 for IES data, and -0.36 ± 0.15 for IMO data). This correlation is statistically non-significant for the IES data while significant (p >.05) for the IMO data. The correlation improves substantially when only the winter months (December, January and February, DJF) are studied (r = -0.41 ± 0.3 and r = -0.42 ± 0.3, respectively) (Table 6.6). This is in agreement with earlier studies by Vinther et al. (2010) that concluded that stable isotope data from SW Greenland are influenced by the North Atlantic Oscillation (NAO) during the winter season. The $\delta^{18}O$ and δD values for both datasets show moderate anti-correlation (r ~ -0.42) to the winter NAO index, however, this relationship is statistically non-significant ($p \geq .05$) (Table 6.6). There is no correlation between *d*-excess values for IES and IMO monthly data when only the winter NAO index is considered (r = 0.17 ± 0.33 and -0.03 ± 0.33, respectively), but significant moderate correlation (r = 0.39 ± 0.15, $p < .05$) is observed between monthly *d*-excess values of IMO samples and the NAO index when the whole dataset is considered (Table 6.6). The correlation between the IES total data and NAO index is weaker and non-significant (r = 0.23 ± 0.15, p = .138). In Figure 6.8, monthly isotopic values for both IES and IMO isotopic data are plotted with the NAO index.

Table 6.6 Linear Regression results (slope and correlation coefficients – r and p-values) between NAO index, IES monthly average and IMO monthly samples , all months and winter months (DJF).

	IES data Total	**IMO data Total**	**IES data DJF**	**IMO data DJF**
$\delta^{18}O$ vs.	-8.06 ± 0.33	-8.53 ± 0.26	-6.68 ± 1.49	-8.18 ± 1.04
NAO index	r = -0.21 ± 0.15	r = -0.36 ± 0.15	r = -0.41 ± 0.3	r = -0.42 ± 0.3
	p = .192	p < .05	p = .209	p = .197
δD vs.	-58.6 ± 2.59	-61.06 ± 2.06	-46.21 ± 11.2	-56.92 ± 8.44
NAO index	r = -0.16 ± 0.16	r = -0.3 ± 0.15	r = -0.42 ± 0.3	r = -0.42 ± 0.3
	p = *.31*	p = .05	p = .204	p = .198
d-excess vs.	5.91 ± 0.58	7.17 ± 0.37	7.21 ± 1.61	8.53 ± 1.05
NAO index	r = 0.23 ± 0.15	r = 0.39 ± 0.15	r = 0.17 ± 0.33	r = -0.03 ± 0.33
	p = .138	p < .05	p = .611	p = .936

The uncertainty on the slope represents the standard deviation and the uncertainty on the correlation coefficient represents the standard error.

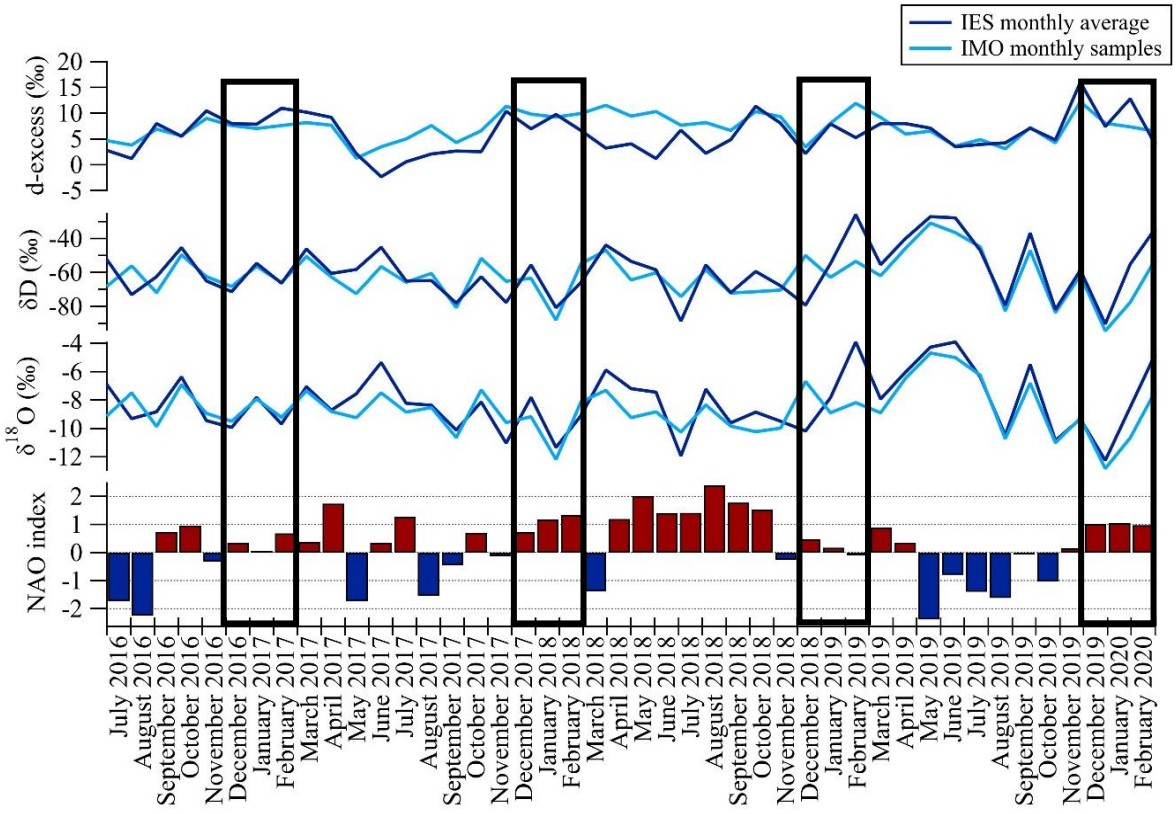

Figure 6.8 Monthly isotopic values plotted with the NAO index, IES monthly average and IMO monthly samples (DJF outlined with black boxes).

Few attempts have been made to reconstruct the NAO index from isotope precipitation data. Vinther, Johnsen, Andersen, Clausen, and Hansen (2003) showed that NAO strongly

influences winter temperatures in Greenland and consequently the isotopic values and the winter NAO index has been shown to significantly correlate to $\delta^{18}O$ in precipitation in Europe (Baldini, McDermott, Foley, & Baldini, 2008; Deininger, Werner, & McDermott, 2016). How winter months are defined can affect the outcome as well, in this study winter months are defined as December to February (DJF), while some studies define winter months from November to April (Wanner et al., 2001). Further observational and modelling studies are necessary to better understand the complex relationship between the atmospheric circulation presented in the NAO index and the isotopic records from Iceland.

7 Conclusions

Precipitation samples were collected in Reykjavík over more than 3 and half-year's period and analyzed for their isotopic content. Some gaps are in the data which is taken into consideration. A database was compiled with results from those measurements as well as results from measurements done at the Institute of Earth Sciences since 2006.

The analyses of the relationship between isotopic and meteorological data reveal that temperature and specific humidity has strong correlation with $\delta^{18}O$ and even stronger anti-correlation to *d*-excess values. Those two are the most important atmospheric controlling factors on the daily precipitation isotope variations in this region. The $\delta^{18}O$ values show weak correlation to precipitation amount, but no correlation is observed between *d*-excess values and precipitation amount. The correlation between $\delta^{18}O$ isotopic values and meteorological variables differ between seasons, with stronger correlation to temperature and specific humidity during winter and spring and strongest correlation to precipitation amount during summer. The correlation between *d*-excess values and temperature and specific humidity is weak during summer but shows strong correlation in all other seasons.

The daily precipitation isotopic composition shows large seasonal variations, with high $\delta^{18}O$ values in the summer and low $\delta^{18}O$ values in the winter, whereas *d*-excess shows an opposite trend, with lower values in the summer and higher values during winter.

The isotopic composition of precipitation has strong variability on short, hourly to daily time scales, within one precipitation event, which potentially could provide valuable information. However, this potential has not yet been fully explored, mainly due to the sparsity of isotope observations with high temporal resolution. The daily sampling also shows a large variability in the isotopic values that is not visible in monthly averages of IES isotope data or the monthly IMO isotope data.

From the comparison between the observed isotope data and the ECHAM5-wiso modelled data it can be concluded that the model is doing a decent job simulating the observed isotopic data, especially when the whole dataset is considered. The model highly overestimates the observed *d*-excess values during summer and fall but underestimates the $\delta^{18}O$ values during winter. The temperature values are underestimated in all seasons by ECHAM5-wiso, especially during spring and summer, while specific humidity is slightly overestimated in all seasons. Precipitation amount is poorly simulated by the model with higher median in all seasons. The model's parametrization of precipitation could be improved by taking into consideration higher resolution isotope data.

Weak anti-correlation is found between the NAO index and the $\delta^{18}O$ values when the whole dataset (42 months) is considered but the correlation improves substantially when only the winter months (December, January and February, DJF) are studied, however those results are statistically non-significant ($p > .05$). No correlation is seen between winter NAO and *d*-excess values. Further observational and modelling studies are necessary to better understand the complex relationship between the atmospheric circulation presented in the NAO index and the isotopic records from Iceland.

7.1 Suggestions for further research

This project has demonstrated the frequent sampling adds to the overall understanding of the isotopic composition of precipitation in the region. It is important that daily sampling of precipitation continues to get a longer time series and thus better constraints on statistical correlation between parameters.

A new precipitation collector has been set up on the other side of the Askja building where daily sampling is taking place simultaneously. This new sampler is further from open surface water and higher from the ground and it will be interesting to see if the different location has any effect on the isotopic outcome. An automatic precipitation sampler, which currently is being constructed at the Institute of Earth Sciences (IES), will give opportunity for more frequent sampling from individual events that will enhance our understanding of isotopic variability on shorter timescale.

A second Picarro analyzer that continuously collects and measures isotopic composition of atmospheric water vapor was installed on top of the Askja building in October 2019, along with a weather station, which gives detailed meteorological information at the sample site. This new setup gives good opportunity to further study the relationship between isotopes within the atmospheric water cycle and meteorological variables and to improve parameterization of the hydrological cycle within isotope-enabled climate models.

References

Aemisegger, F., Spiegel, J., Pfahl, S., Sodemann, H., Eugster, W., & Wernli, H. (2015). Isotope meteorology of cold front passages: A case study combining observations and modeling. *Geophysical Research Letters, 42*(13), 5652-5660.

Balagizi, C. M., Kasereka, M. M., Cuoco, E., & Liotta, M. (2018). Influence of moisture source dynamics and weather patterns on stable isotopes ratios of precipitation in Central-Eastern Africa. *Science of The Total Environment, 628*, 1058-1078.

Baldini, L. M., McDermott, F., Foley, A. M., & Baldini, J. U. (2008). Spatial variability in the European winter precipitation δ18O-NAO relationship: Implications for reconstructing NAO-mode climate variability in the Holocene. *Geophysical Research Letters, 35*(4).

Bedaso, Z., & Wu, S.-Y. (2020). Daily precipitation isotope variation in Midwestern United States: Implication for hydroclimate and moisture source. *Science of The Total Environment*, 136631.

Bony, S., Colman, R., Kattsov, V. M., Allan, R. P., Bretherton, C. S., Dufresne, J.-L., Hall, A., Hallegatte, S., Holland, M. M., Ingram, W., Randall, D. A., Soden, B. J., Tselioudis, G., & Webb, M. J. (2006). How well do we understand and evaluate climate change feedback processes? *Journal of Climate, 19*(15), 3445-3482.

Bowen, G. J., & Wilkinson, B. (2002). Spatial distribution of δ18O in meteoric precipitation. *Geology, 30*(4), 315-318.

Celle-Jeanton, H., Gonfiantini, R., Travi, Y., & Sol, B. (2004). Oxygen-18 variations of rainwater during precipitation: application of the Rayleigh model to selected rainfalls in Southern France. *Journal of Hydrology, 289*(1-4), 165-177.

Clark, I. D., & Fritz, P. (2013). *Environmental isotopes in hydrogeology*: CRC press.

Craig, H. (1961). Isotopic variations in meteoric waters. *Science, 133*(3465), 1702-1703.

Dansgaard, W. (1953). The abundance of O18 in atmospheric water and water vapour. *Tellus, 5*(4), 461-469.

Dansgaard, W. (1964). Stable isotopes in precipitation. *Tellus, 16*(4), 436-468.

Deininger, M., Werner, M., & McDermott, F. (2016). North Atlantic Oscillation controls on oxygen and hydrogen isotope gradients in winter precipitation across Europe; implications for palaeoclimate studies. *Climate of the Past, 12*(11), 2127-2143.

Einarsson, M. A. (1984). Climate of Iceland. *World survey of climatology, 15*, 673-697.

Froehlich, K., Gibson, J., & Aggarwal, P. (2002). *Deuterium excess in precipitation and its climatological significance*. Retrieved from

Fujita, K., & Abe, O. (2006). Stable isotopes in daily precipitation at Dome Fuji, East Antarctica. *Geophysical Research Letters, 33*(18).

Gat, J. R., Mook, W. G., & Meijer, H. A. (2001). Environmental isotopes in the hydrological cycle. *Principles and Applications UNESCO/IAEA Series, 2*, 63-67.

Geyh, M. (2000). *Environmental isotopes in the hydrological cycle: Groundwater - Saturated and unsaturated zone*. Retrieved from International Atomic Energy Agency and United Nations Educational, Scientific and Cultural Organization, Vol. IV.:

Gonfiantini, R., Roche, M.-A., Olivry, J.-C., Fontes, J.-C., & Zuppi, G. M. (2001). The altitude effect on the isotopic composition of tropical rains. *Chemical Geology, 181*(1-4), 147-167.
Held, I. M., & Soden, B. J. (2006). Robust responses of the hydrological cycle to global warming. *Journal of Climate, 19*(21), 5686-5699.
Ichiyanagi, K. (2007). Studies and applications of stable isotopes in precipitation. *Journal of Japanese association of hydrological sciences, 37*(4), 165-185.
Já. (2020). Kort - Loftmynd af Reykjavík - OpenStreetMap. Retrieved from https://ja.is/kort/?x=357022&y=406774&nz=13.49
Johnsen, S., Dansgaard, W., & White, J. (1989). The origin of Arctic precipitation under present and glacial conditions. *Tellus B: Chemical and Physical Meteorology, 41*(4), 452-468.
Kendall, C., & Doctor, D. H. (2003). Stable Isotope Applications in Hydrologic Studies. In J. I. (Ed.), *Treatise on Geochemistry*.
Knauer, J., El-Madany, T. S., Zaehle, S., & Migliavacca, M. (2018). Bigleaf—An R package for the calculation of physical and physiological ecosystem properties from eddy covariance data. *PloS one, 13*(8).
Merlivat, L., & Jouzel, J. (1979). Global climatic interpretation of the deuterium-oxygen 18 relationship for precipitation. *Journal of Geophysical Research: Oceans, 84*(C8), 5029-5033.
Mook, W., & Rozanski, K. (2000). Environmental isotopes in the hydrological cycle. *IAEA Publish, 39*.
Muller, C. L., Baker, A., Fairchild, I. J., Kidd, C., & Boomer, I. (2015). Intra-event trends in stable isotopes: Exploring midlatitude precipitation using a vertically pointing micro rain radar. *Journal of Hydrometeorology, 16*(1), 194-213.
NASA. (2016). Temperature Over Time - The Oxygen and Hydrogen Isotope Ratio. Retrieved from http://www.ces.fau.edu/nasa/module-3/how-is-temperature-measured/isotopes.php
NASA. (2019). MODIS Rapid Response Project at NASA/GSFC. Retrieved from https://lance.modaps.eosdis.nasa.gov/gallery/
NOAA. (2020). A record of NAO phases for 1950 through the present. Retrieved from ftp://ftp.cpc.ncep.noaa.gov/wd52dg/data/indices/tele_index.nh
Pfahl, S., & Sodemann, H. (2014). What controls deuterium excess in global precipitation? *Climate of the Past, 10*(2), 771-781.
Pfahl, S., Wernli, H., & Yoshimura, K. (2012). The isotopic composition of precipitation from a winter storm: A case study with the limited-area model COSMOiso. *Atmospheric Chemistry and Physics, 12*(3), 1629-1648.
Picarro. (2019). Cavity Ring-Down Spectroscopy (CRDS). Retrieved from http://www.picarro.com/technology/cavity_ring_down_spectroscopy
Risi, C., Bony, S., & Vimeux, F. (2008). Influence of convective processes on the isotopic composition (δ18O and δD) of precipitation and water vapor in the tropics: 2. Physical interpretation of the amount effect. *Journal of Geophysical Research: Atmospheres, 113*(D19).
Roeckner, E., Bäuml, G., Bonaventura, L., Brokopf, R., Esch, M., Giorgetta, M., Hagemann, S., Kirchner, I., Kornblueh, L., & Manzini, E. (2003). The atmospheric general circulation model ECHAM 5. PART I: Model description.
Rozanski, K., Araguás-Araguás, L., & Gonfiantini, R. (1993). Isotopic patterns in modern global precipitation. *Climate change in continental isotopic records, 78*, 1-36.

Science, G. (2019). Regional Factors – Water. Retrieved from https://www.gns.cri.nz/Home/Our-Science/Environment-and-Materials/Authentication-Studies/Analytical-Techniques/Stable-Isotopes/Regional-Factors-Water
Sharp, Z. (2017). Principles of stable isotope geochemistry.
Sjostrom, D. J., & Welker, J. M. (2009). The influence of air mass source on the seasonal isotopic composition of precipitation, eastern USA. *Journal of Geochemical Exploration, 102*(3), 103-112.
Sodemann, H. (2006). *Tropospheric transport of water vapour: Lagrangian and Eulerian perspectives*: ETH Zurich.
Soderberg, K., Good, S. P., O'Connor, M., Wang, L., Ryan, K., & Caylor, K. K. (2013). Using atmospheric trajectories to model the isotopic composition of rainfall in central Kenya. *Ecosphere, 4*(3), 1-18.
Steen-Larsen, H. C. (2018). Program to analyze Picarro data.
Steen-Larsen, H. C., Risi, C., Werner, M., Yoshimura, K., & Masson-Delmotte, V. (2017). Evaluating the skills of isotope-enabled general circulation models against in situ atmospheric water vapor isotope observations. *Journal of Geophysical Research: Atmospheres, 122*(1), 246-263.
Stocker, T., Qin, D., Plattner, G., Tignor, M., Allen, S., Boschung, J., Nauels, A., Xia, Y., Bex, V., & Midgley, P. (2013). IPCC, 2013: summary for policymakers in climate change 2013: the physical science basis, contribution of working group I to the fifth assessment report of the intergovernmental panel on climate change. *Camb. Univ. Press Camb. UKNY NY USA*.
Sveinbjörnsdóttir, Á., Johnsen, S., & Arnórsson, S. (1995). *The use of stable isotopes of oxygen and hydrogen in geothermal studies in Iceland.* Paper presented at the World Geothermal Congress.
Taylor, K. E. (2001). Summarizing multiple aspects of model performance in a single diagram. *Journal of Geophysical Research: Atmospheres, 106*(D7), 7183-7192.
Team, R. C. (2013). R: A language and environment for statistical computing.
Thermo-Fisher. (2019). GasBench II - Universal On-Line Gas Preparation and Introduction System for Isotope Ratio MS. In.
Thomas, R. (2013). *Practical guide to ICP-MS: a tutorial for beginners*: CRC press.
U.S. Geological Survey. (2013). Scematics of mass spectrometer. Retrieved from http://pubs.usgs.gov/of/2001/ofr01-257/images/figure1.gif
Veðurstofa Íslands. (2018). Tíðarfar ársins 2017. Retrieved from https://www.vedur.is/um-vi/frettir/tidarfar-arsins-2017-1
Veðurstofa Íslands. (2019a). Combined Infrared (AVHRR/SEVIR) thermal satellite image and reflection from weather radar in Iceland. In.
Veðurstofa Íslands. (2019b). Hiti í 2m hæð/Temperature in 2m (°C). In hm750m_sv_2t_2019091806 (Ed.).
Veðurstofa Íslands. (2019c). Spákort gert á VÍ - ECHWF/ECM: 18.09.2019 06Z. In.
Veðurstofa Íslands. (2019d). Tíðarfar ársins 2018. Retrieved from https://www.vedur.is/um-vi/frettir/tidarfar-arsins-2018
Veðurstofa Íslands. (2019e). Veðurfarsyfirlit - Reykjavík júní 2019. Retrieved from https://www.vedur.is/media/vedurstofan/utgafa/hlidarefni/climat/climat-Reykjavik-6-2019.pdf
Vinther, B. M., Johnsen, S. J., Andersen, K. K., Clausen, H. B., & Hansen, A. W. (2003). NAO signal recorded in the stable isotopes of Greenland ice cores. *Geophysical Research Letters, 30*(7).

Vinther, B. M., Jones, P., Briffa, K., Clausen, H., Andersen, K. K., Dahl-Jensen, D., & Johnsen, S. (2010). Climatic signals in multiple highly resolved stable isotope records from Greenland. *Quaternary Science Reviews, 29*(3-4), 522-538.

Visbeck, M. H., Hurrell, J. W., Polvani, L., & Cullen, H. M. (2001). The North Atlantic Oscillation: past, present, and future. *Proceedings of the National Academy of Sciences, 98*(23), 12876-12877.

Vuille, M. (2018). Current state and future challenges in stable isotope applications of the tropical hydrologic cycle (Invited Commentary). *Hydrological Processes, 32*(9), 1313-1317.

Wanner, H., Brönnimann, S., Casty, C., Gyalistras, D., Luterbacher, J., Schmutz, C., Stephenson, D. B., & Xoplaki, E. (2001). North Atlantic Oscillation–concepts and studies. *Surveys in geophysics, 22*(4), 321-381.

Wassenaar, L., Terzer-Wassmuth, S., Douence, C., Araguas-Araguas, L., Aggarwal, P., & Coplen, T. B. (2018). Seeking excellence: An evaluation of 235 international laboratories conducting water isotope analyses by isotope-ratio and laser-absorption spectrometry. *Rapid Communications in Mass Spectrometry, 32*(5), 393-406.

Werner, M., Langebroek, P. M., Carlsen, T., Herold, M., & Lohmann, G. (2011). Stable water isotopes in the ECHAM5 general circulation model: Toward high-resolution isotope modeling on a global scale. *Journal of Geophysical Research: Atmospheres, 116*(D15).

World Meteorological Organization. (2020). World Weather Information Service - Reykjavík. Retrieved from http://worldweather.wmo.int/en/city.html?cityId=189

Xi, X. (2014). A review of water isotopes in atmospheric general circulation models: recent advances and future prospects. *International Journal of Atmospheric Sciences, 2014*.